FABRICATION OF NdFeB THIN FILM FOR APPLICATION IN SUPERCONDUCTOR AND FERROMAGNETIC HYBRID SYSTEMS AND CHARACTERIZATION BY USING LOW TEMPERATURE SCANNING HALL PROBE MICROSCOPY

by

Sunusi Suleiman USMAN

A thesis submitted to

the Graduate Institute of Science and Engineering

of

Meliksah University

in partial fulfilment of the requirement for the degree of

Master of Science

in

Electrical and Computer Engineering

June 2014
Kayseri, Turkey

APPROVAL PAGE

This is to certify that I have read the thesis entitled "Fabrication of NdFeB Thin Film for Application in superconductor and Ferromagnetic Hybrid Sytems and Characterization by using Low Temperature Scanning Hall Probe Microscopy" by Sunusi Suleiman USMAN and that in my opinion it is fully adequate, in scope and quality, as a thesis for the degree of Master of Science in Electrical and Computer Engineering, the Graduate Institute of Science and Engineering, Melikşah University.

$$\overline{\hspace{4cm}}$$

June 5, 2014   Yrd. Doç . Dr. A. Esad ÖZMETIN
                                     Supervisor

I certify that this thesis satisfies all the requirements as a thesis for the degree of Master of Science.

$$\overline{\hspace{4cm}}$$

June 5, 2014   Prof. Dr. Murat UZAM
                                 Head of Department

Examining Committee Members
Title and Name   Approved

Prof. Dr. Halidun KELEŞTEMUR   June 5, 2014   _____

Yrd. Doç. Dr. Gökhan ÖZGÜR   June 5, 2014   _____

Yrd. Doç. Dr. Kadir.A.PEKER   June 5, 2014   _____

Yrd. Doç. Dr. Ali Esad ÖZMETIN   June 5, 2014   _____

It is approved that this thesis has been written in compliance with the formatting rules laid down by the Graduate Institute of Science and Engineering.

$$\overline{\hspace{4cm}}$$

Prof. Dr. M. Halidun KELEŞTEMUR
Director

ABSTRACT

FABRICATION OF NdFeB THIN FILM FOR APPLICATION IN SUPERCONDUCTOR AND FERROMAGNETIC HYBRID SYSTEMS AND CHARACTERIZATION BY USING LOW TEMPERATURE SCANNING HALL PROBE MICROSCOPY

Sunusi Suleiman USMAN

M.S Thesis Electrical and Computer Engineering
June 2014

Supervisor: Assist. Prof. Dr. Ali Esad ÖZMETIN

ABSTRACT

A review and experimental investigation were realized in this study. The review includes permanent magnets, the fabrication as well as the image processing techniques.In this experimental study, samples were prepared by RF sputtering from the home-made NdFeB target and a target of Mg was used to remove oxygen from silicon substrate at room temperature condition. CuTEM with 1500 square mesh was used as a shadow mask to pattern the film surface. Films were capped with few thick nanometer tantalum layers against diffusion and oxidation. The liquid nitrogen cold finger was added periodically during the sputtering process to ensure trapping of the impurities in the system. The films were thermally annealed at 550 ℃ for 30 minutes. X-ray diffraction pattern was performed for both non-annealed and annealed temperature as grown sample and formation of $Nd_2Fe_{14}B$ phase was realized during an x-ray diffraction investigation with good lattice orientation.We have imaged the sample surface with the aid of the low temperature SHPM system to be used for determining the scanning image of the sample surface at various temperatures.This allows the experimental investigation to acquire a topographical image along with the field distribution which was achieved.The image results then show that the scanning images with SHPM give a better smooth image and are well complimented.The film which was studied can be used for applications in superconductor and ferromagnetic hybrid structures.

Keywords: Neodymium-Iron-Boron, Sputtering Techniques, Low Temperature Scanning Hall Probe Microscopy.

ÖZ

SÜPERİLETKEN VE FERROMANYETİK HİBRİT SİSTEM UYGULAMALARI İÇİN NdFeB İNCE FİLM ÜRETİMİ VE DÜŞÜK SICAKLIK HALL PROBE GÖRÜNTÜLEMESİ İLE KARAKTERİZASYONU

Sunusi Suleiman USMAN

Yüksek Lisans Tezi – Elektrik – Bilgisayar Mühendisliği
Haziran 2014

Tez Yöneticisi: Yrd. Doç. Dr. A. Esad ÖZMETİN

ÖZ

Bu çalışmada deneysel incelemeler gerçekleştirilmiştir. Çalışma, kalıcı mıknatıslanma için manyetik malzemelerin üretim tekniklerinin yanı sıra görüntü işleme tekniklerini de içerir. Bu deneysel çalışmada kullanılan örnekler, el yapımı NdFeB target kullanılarak RF püskürtme yöntemiyle hazırlandı ve başka bir Mg target yardımı ile oda sıcaklığında silikon altlık üzerinde oksijenin tutulması sağlandı. Film yüzeyini örnek almak amacıyla CuTEM 1500 kare şeklindeki bir gölge maske kullanılmıştır. Daha sonra filmler oksijen ve oksidasyona karşı bir nanometre kalınlığında Tantalum tabakası tarafından kapatılmıştır. Film kaplama işlemi sürerken sıvı azot kullanılarak sistemin içerisindeki empüriteler soğuk hazne bölümünde toplanarak engellenmiş ve püskürtme işlemi sırasında düzenli aralıklarla sıvı azot ilavesine devam edilmiştir. Bu filmler 30 dakika süre ile termal olarak 550 ℃ de tavlanmıştır. Tavlanmış ve tavlanmamış $Nd_2Fe_{14}B$ filmlerin X-Işını kırınım grafikleri elde edilmiştir. Oda sıcaklığının değişken değerlerinde Hall Probe tarama mikroskobisi yardımıyla yüzey görüntüleri alınmıştır. Bu çalışmada aynı zamanda yüzey topografisi ve manyetik alan dağılım haritası da elde edilmiştir. SHPM görünüleme sonuçları bize film yüzeyinin ne kadar pürüzsüz ve kullanışlı olduğunu göstermiştir. Sonuç olarak elde edilen filmin, süperiletken ve ferromanyetik hibrid sistemler için kullanılabilir olduğu anlaşılmıştır.

Anahtar Kelimeler: Neodmium-Demir-Boron, Püskürtme Teknikleri, Düşük Sıcaklık Hall Probe Tarama Mikroskopisi.

DEDICATION

I dedicate this project to my able Governor Engr. Dr. Rabiu Musa Kwankwaso

ACKNOWLEDGEMENT

. For the beatific and beautiful beginning, infinite thanks be to Almighty Allah who gave me the wisdom to carry out this task, and may the benediction and salutation of Allah be upon the Head messenger prophet Mohammad (p.b.h) who reads or write not.

I express sincere gratitude to my supervisor Assist. Prof. Dr. A. Esad OZMETIN

for his endless support and kind of gesture throughout the research.

I express my thanks to Mr. Mehmet KURU and Mr. Erhan ONUGUN for their guidance and understanding throughout the research.

Also, my gratitude goes to my family and Engr. Abubakar Adamu WARA who made me stay at the University for their support, love and care they gave to me.

The responsibility for this project was entirely mine, and any credit I happily share with all those mentioned above is of free will.

TABLE OF CONTENTS

LIST OF TABLES

TABLE

LIST OF FIGURES

FIGURE

SYMBOLS AND ABBREVIATIONS

SYMBOL/ ABBREVIATION

F_3O_4	Iron three-four Oxide
O^{2-}	Oxygen- ion two- negative
S_mCO_5	Samarium-Cobalt five
$\dot{A}$	Angstrom
Al_2O_3	Aluminium-Oxide
$\dot{A}/s$	Angstrom-per- second
Al-Ni-Co	Aluminium-Nickel-Cobalt
℃	Degree of Temperature
Cu-Ni-Fe	Copper-Nickel-Iron
K	Kelvin
$K\dot{A}$	Kilo-Angstrom
Kj/m^3	Kilojoule per metre cube
Mn^{2+}	Manganese-ion two- positive
Mg	Magnesium
MnO	Manganese-Oxide
$Nd_2Fe_{14}B$	Neodymium-Iron-Boron phase
NdFeB	Neodymium-Iron-Boron
Oe	Oersted
$\gamma - F_2O_3$	Gama-Iron two-three Oxide
$\mu m/s$	Micrometer-per-Second
$\Omega.m$	Ohm-meter
μmA	Micrometer-Ampere
μ_o	Permeability

2DEG	Two-Dimensional-Electron-Gas
AFM	Atomic-Force-Microscopy
Amp/t/m	Ampere-per-turn-per-metre
Ar	Argon
BD	Bitter-Decoration
EM	Electron-Microscopy
Hc	Coercivity
I	Current
KHZ	Kilo-Hertz
KOe	Kilo-Oersted
KV	Kilo-Voltage
Max	Maximum
MO	Magnetic-Optical-Imaging-Microscopy
Ms	Saturation-Magnetization
Ns	Nano-second
PVD	Physical-Vapor-Deposition
SHPM	Scanning-Hall-Probe-Microscope
Si	Silicon
SJJM	Scanning-Josephson-Junction-Microscopy
SNRs	Signal-to-Noise-Ratio
SQUID	Scanning-Superconducting-Interface Device
STM	Scanning-Tunneling-Microscope
T	Tesla
V	Voltage
W	Watt
Wt%	Weight in percentage

CHAPTER 1

INTRODUCTION

Magnets have become one of the essential needs of human invention for over a long period of time. Early magnet used as lodestone application of affine mixture of ferrimagnetic magnetite (Fe_3O_4) and anti-ferromagnetic maghemite ($\gamma - Fe_2O_3$), in geometry and in compasses by Chinese experts is well documented [1].With the advancement of magnets, they have come to play a vital role in our society, particularly in the growth of innovative technology. Today applications of magnets ease human activities because of the high demand in the market place. People are highly influenced as the costs of effectiveness are improved and their magnetic properties are very coercive. Magnets are the necessities for high motor operations in our industrial applications; these include all actuators, DC Motors, sensors, magnetic resonance imaging, magnetic cranes, roller coasters, car doors, hard-disk drives and many others [2].

Alinco magnets were some of the first magnetic materials produced.These were made up of aluminium, nickel and cobalt compared to today's standard ones, which have poor magnetic properties, but overall good temperature properties.Ceramic and ferrite magnets were developed in the early 1950s. These are what are more commonly found on refrigerators today. The 1960s saw the creation of samarium cobalt magnet which had the highest energy product of any magnetic material. Due to an increase in the cost of cobalt there began a large push for an iron based permanent magnet. Soon after, in the 1980s neodymium-iron-boron magnets were developed with largest energy product [3]. Numerous studies have been conducted to understand, the better knowledge of Nd-Fe-B film. Most of this research was carried out on bulk of NdFeB and only a few works related to neodymium iron boron film material. Today, with the rapid increase of permanent magnets, magnets are playing a vital role in modern technological application both in industry and research area.

Nd-Fe-B magnets are greatly sensitive to its microstructure.In bulk materials, the microstructure comprising of a uniform distribution of aligned $Nd_2Fe_{14}B$ grains enclosed by a non-magnetic Nd-rich grain boundary phase is preferred for higher performance. For thin films, fine microstructure as well as out of plane texture is needed to attain high energy product. Sputtering is one of the possible ways to prepare anisotropic N-Fe-B thin films. During sputtering, the microstructure and texture of the $Nd_2Fe_{14}B$ phase are moved by a number of processing parameters such as deposition rate, temperature, vacuum condition and buffer layer [4].

The aim of this experimental investigation is to fabricate Nd-Fe-B thin film by sputtering techniques. The sample is to be investigated by using X-ray diffraction analysis to obtain information on the atomic scale as well as the structural information of $Nd_2Fe_{14}B$ and its orientation. Furthermore, a low temperature scanning Hall probe microscopy system which has different tracking modes is to be used in obtaining the image of the sample surface.The films to be obtained can be used for applications in superconductor and ferromagnetic hybrid systems.

CHAPTER 2

MAGNETIC MATERIAL

2.1 MAGNETIC ORIGIN

Magnet originates from magnetic field with magnetic moment along its axis of rotation that two sources were generated and the orbital motion around the nucleus as shown in Fig. 2.1a; and the other which is a moving charge electron in a spin direction around the current loop as shown in Fig. 2.1b which acts as a permanent orbital and spin magnetic moments [5].
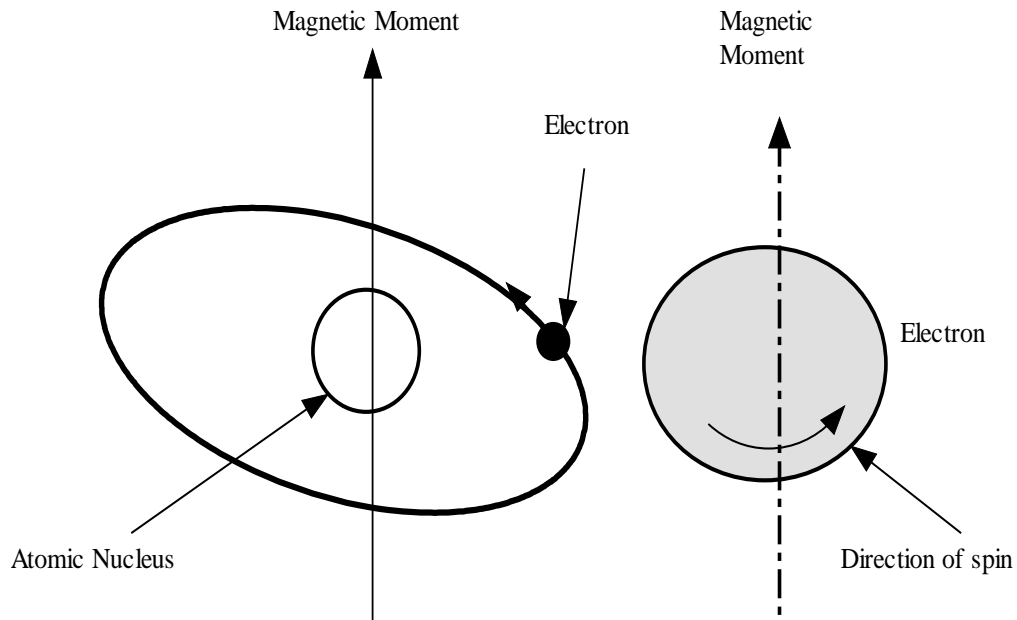
Fig 2.1 a) Magnetic moment with an orbital electron. b) Magnetic moment with a spin direction [5].

2.2 MAGNETISM

Magnetism refers to the occurrence or a trend where irons attract or repel onto each other as a result of magnetic force or by a moving electric current. However, the important principles and techniques explain the magnetic trend are multifaceted. So its understanding has dodged scientists until relatively recent time. Today's technologically oriented gadgets are dependent upon magnetism and magnetic substance; some of which power generating plants, transformers, electric motors, TV sets, computer systems, recording systems etc. This magnetism includes the following types of magnetism as diamagnetism, paramagnetism and ferromagnetism. All magnetic materials constitute one of these types and the actions depend on the reaction of electron and atomic dipoles (pair of opposite poles) to the application of an external applied magnetic field. Fig.2.2a shows the schematic diagram of the atomic magnetic dipole alignment for a diamagnetic material with and without an external magnetic field by an arrow to represent the atomic dipole moment. Fig 2.2b shows magnetic dipole acting independently without being reciprocated by nearby dipole with external field they enhanced [5].
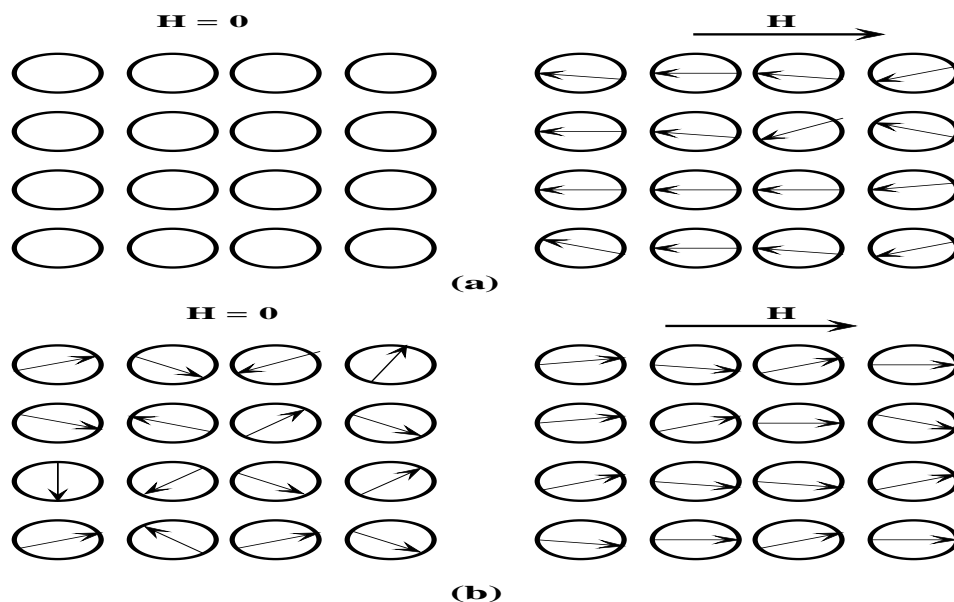
Fig. 2.2 a) Diamagnetic with and without a magnetic field and no dipole exists. b) Paramagnetic with and without an external magnetic field [5].

2.2.1 Ferromagnetism

Some metallic materials hold a permanent magnetic moment in the absence of an external field and evident of very large and permanent magnetization shows presence. Permanent magnetic moments due to uncancelled electron spins as a result of the electronic structure and they are displayed by transition metals, iron (as BCC γ-Ferrite), cobalt, nickel and some of the rare earth metal. Magnetic susceptibilities as high as 10^6 are possible in ferromagnetic materials, and coupling interactions cause a net spin magnetic moment of adjacent to align with one another. As in Fig.2.3, the mutual alignment of atomic dipoles of atomic for a ferromagnetic material will exist even in the absence of an external magnetic field [5].

$$H = 0$$
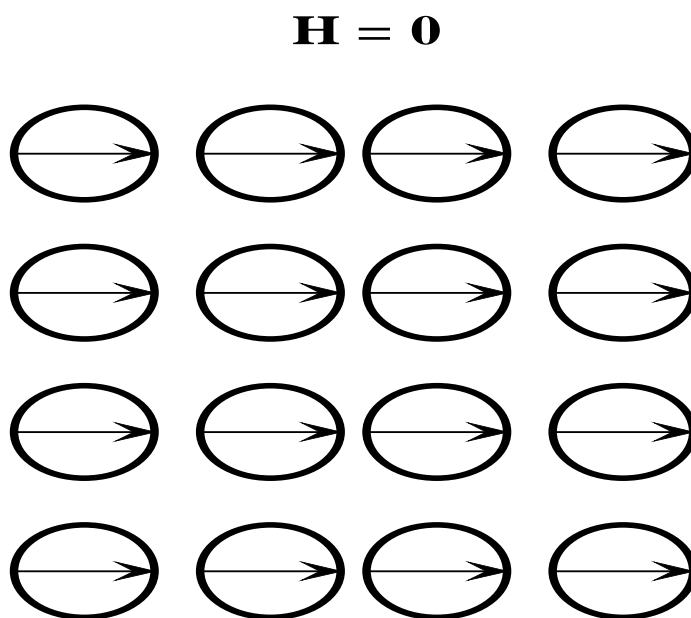
Fig.2.3. Schematic diagram of mutual alignment of atomic dipole for a ferromagnetic [5].

This shows that, $H \ll M$ and therefore the equation it said to be approximately $B \cong \mu_0 M$. The highest promising saturation magnetization M_S of ferromagnetic material symbolises the magnetization. The results when all magnetic dipoles are in solid, equally arrange in a line with outside field; the saturation flux density B_S is, therefore the resultant force [5].

2.2.2 Anti-Ferromagnetism

This occurrence of magnetic moment coupler between near atoms or ions occurs in materials which are further than that of ferromagnetic. This ferromagnetism has coupling results as shown in Fig.2.4 in anti-parallel alignment, the alignment of the spin motion of surrounding atoms or ions in exactly opposite direction is named antiferromagnetism. Manganese oxide (Mno) is one material that shows this behavior. Manganese oxide is a ceramic material that is ionic in character having both Mn^{2+} and O^{2-} ions. No net magnetic moment associated with the O^{2-} ions happens, because there is total cancellation of both spin and orbital moment [5].

$$Mn^{2+} \qquad O^{2-}$$
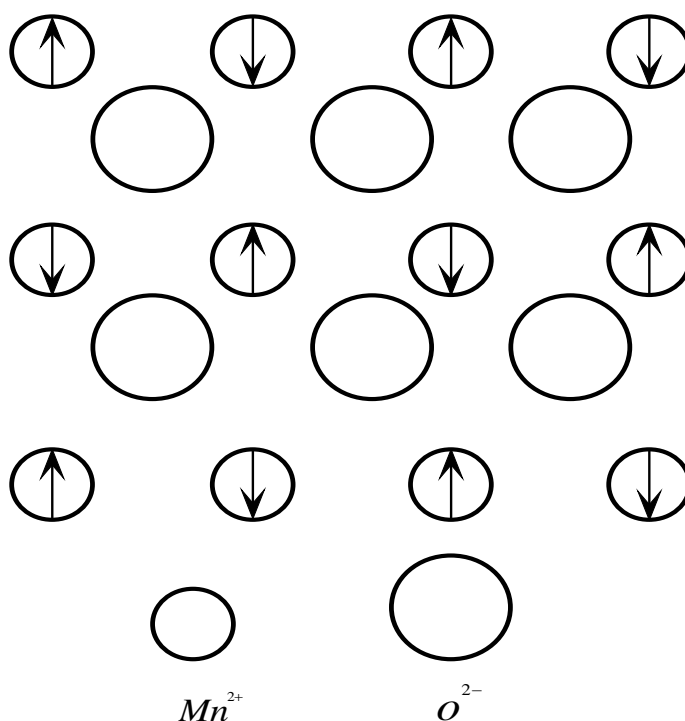
Fig.2.4 Schematic representation of the antiparallel alignment of spin magnetic moments for antiferromagnetic manganese oxide [5].

2.3 DOMAIN AND HYSTERESIS

For any ferromagnetic or ferrimagnetic material, temperature below Tc consists of small volume region when there is a mutual alignment in the same direction of all magnetic dipole moments, each of which is magnetized to its saturation magnetization, and with such a region it is called a domain. Typically, these domains are microscopic in size and all may have different magnetization arrangements. Fig.2.5 shows how hysteresis effect is produced when the B field lags behind the applied H field or decreases at a lower rate. A negative coercivity must be applied in a direction opposite to that of the original field called the coercivity Hc by reducing the B field enclosed to the specimen to zero, and at zero H field there exists a residual field called remanence [5].
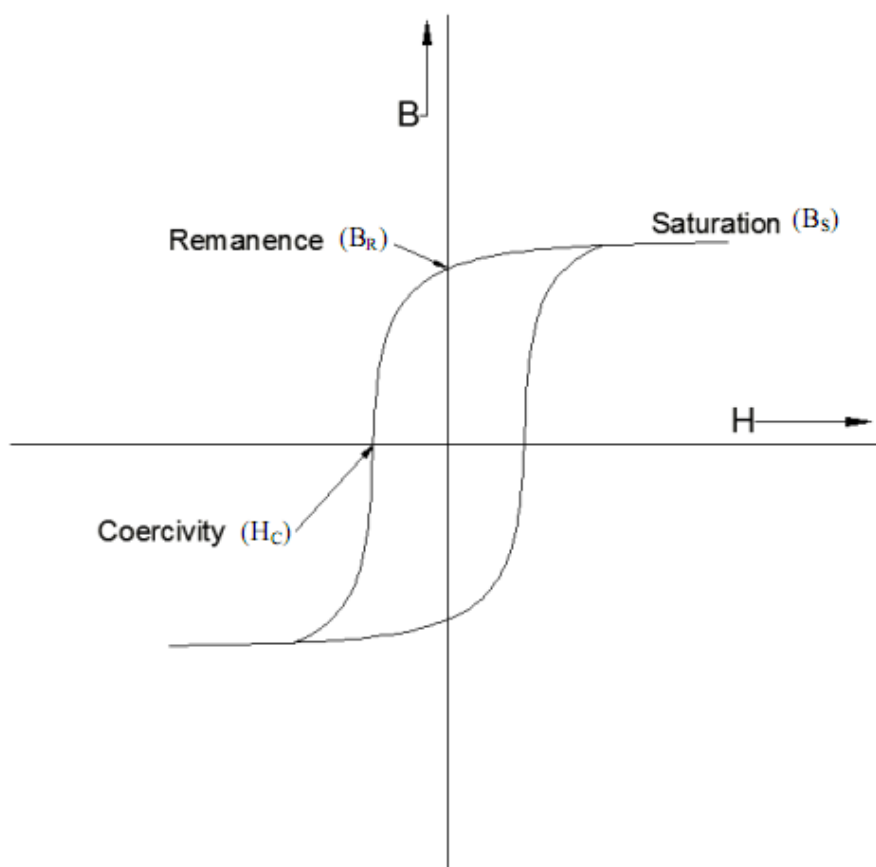
Fig.2.5 The importance of ferromagnetic hysteresis loop [3].

2.4 HARD MAGNETIC MATERIAL

Hard magnetic materials are used in permanent magnets which must have a high coercivity, a high remanence, resistance to demagnetization and a low initial permeability as well as high hysteresis energy losses and saturation flux density. The hysteresis presences of soft and hard magnetic material are compared in Fig.2.6. The two most important appearances relative to the application of these materials are energy product designated as (B-H) max and what is termed as coercivity. The larger (B-H) max the harder the material is in terms of its magnetic characteristics, the value of the energy product is characteristic of the energy required to demagnetize a permanent magnet [5].
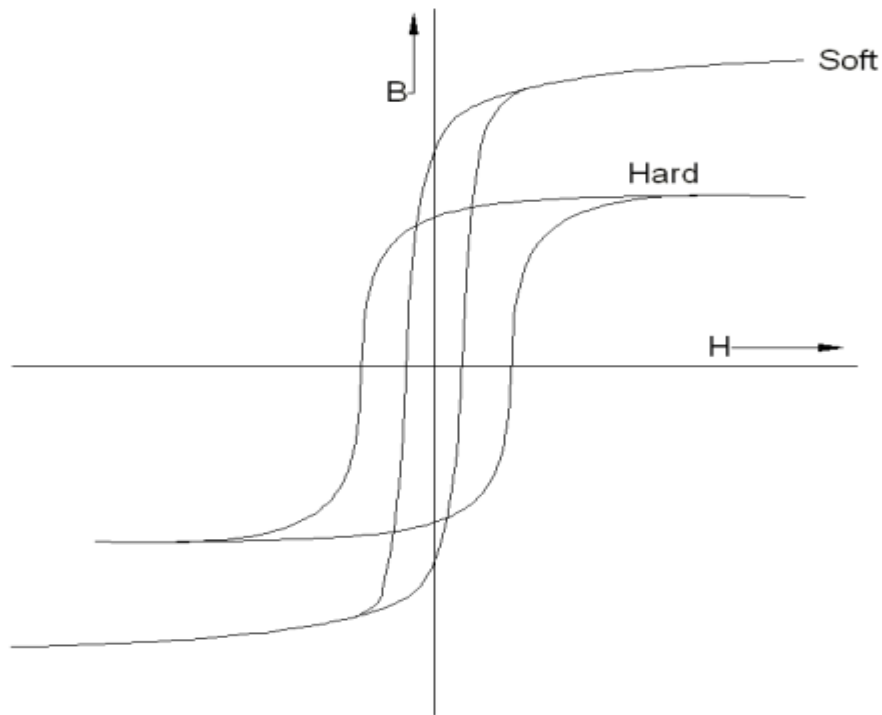
Fig. 2.6 Schematic magnetization curves for soft and hard magnetic material [3].

2.4.1 Conventional Hard Magnetic Material

Hard magnetic materials fall within two main domains, conventional and high energy. In conventional, materials have (B-H) max value that ranges between about 2 and 80 kJ/m^3. These include ferromagnetic materials, magnet steels, Cunife (Cu-Ni-Fe) alloys, Alnico (Al-Ni-CO) and they have an appropriate heat treatment form tremendously small single-domain and strongly magnetic iron-cobalt particles within a nonmagnetic matrix phase [5].

2.4.2 High-Energy Hard Magnetic Material

Permanent magnetic materials require energy production in excess of about 80 kJ/m^3 which is considered to be of the high energy type. These recently developed intermetallic compounds that have a variety of compositions. The two that have found commercial exploitation are $SmCO_5$ and $Nd_2Fe_{14}B$. These high-energy hard magnetic materials are employed in different devices in a variety of technology field. One common application is in the motor [5].

Table 2.1 Magnetic properties of common material [5].

Materials	Composition (Wt %)	Remance Br (Tesla)	Coerciviy Hc(amp/turn/m)	(BH) max KJ/m^3	Curie Temp[°C(k)]	Resistivity ρ (Ω.m)
CuNiFe	20Fe,20Ni,60 CU	0.54	44,000	12	410	$1.8E^{-7}$
Sintered $AlNiCO_8$	34Fe,7Al	0.76	125,000	36	860	-
Cobalt rare earth	$SmCO_5$	0.92	72,000	170	720	$5.0E^{-7}$
Sintered NdfeB	$Nd_2Fe_{14}B$	1.16	848,000	255	$310 - 583$	$1.6E^{-6}$

2.5 NEODYMIUM-IRON-BORON

Samarium is an unreliable and relatively expensive material; furthermore the price of cobalt is variable and its sources are erratic [5]. The effort to find better and /or cheaper permanent magnet materials led to two essentially simultaneous discoveries of $Nd_2Fe_{14}B$, a previously unknown tetragonal crystal with strong uniaxial anisotropy and curie temperature slightly above 300℃ [6]. The principal disadvantages of the Nd-Fe-B family are relatively low Curie temperature near 300℃, which means a fairly strong temperature dependence of magnetic properties at room temperature and susceptibility to severe corrosion in moist atmosphere. The corrosion problems are largely overcome with various metallic and non-metallic coatings [6]. The Fig.2.7 shows the structure of NdFeB and how the atoms are arranged in layers which are embedded in the matrix grain and it comprises 68 atoms with lattice parameter of unit cell. The crystal of the intermetallic compound constitutes the NdFeB magnet. The structure in which the neodymium atoms are between the layer that iron atom form produces superior magnetic properties and boron which is a mere 1% of the weight is thought to be effective in raising the Curie temperature.
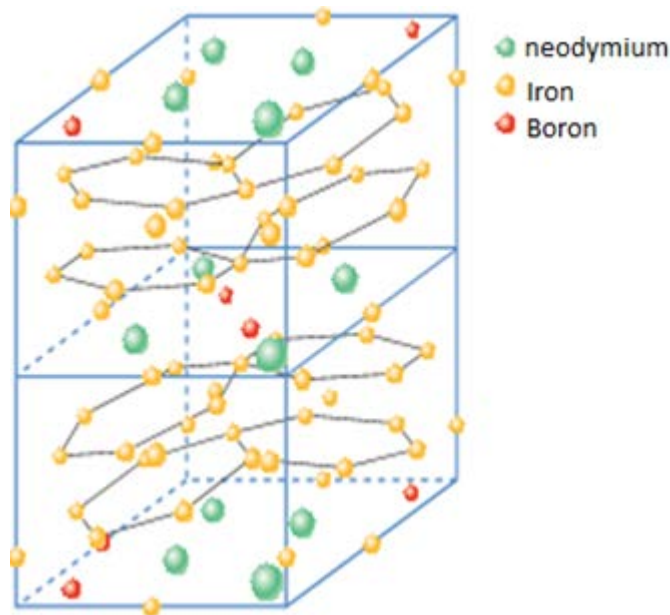
Fig.2.7 Structure of Nd-Fe-B (courtesy japan prize "environment, energy and infrastructure") [5].

2.5.1 Nd-Fe-B Thin Films

A study shows that the fabrication of Nd-Fe-B thin films was firstly demonstrated by Cadieu Cheung and Wickramasekara1986. They prepared Nd-Fe-B films using a slow deposition rate together with applying bias field in the in-plane direction and high H_c of 16 KOe was achieved. However, in order to consider a practical use, some drawbacks were pointed out. The substrate temperature during deposition, 750 ℃ was too high and the easy magnetization axis was aligned in the in-plane direction, since then, many studies have been made in order to control the crystal orientation and to improve the magnetic properties [7].

With the easy magnetic axis perpendicular to the substrate, deposition parameters such as temperature, composition, and especially the thickness change. It is possible to control the phase formation, texture, and grain sizes, and thus to optimize the coercivity and magnetic texture [8]. The $Nd_2Fe_{14}B$ phase providing the desired intrinsic magnetic properties has a tetragonal unit cell (a = 8.85Å, c = 12.30Å) and it comprises 68 atoms [9]. The high perpendicular magnetic anisotropy of $Nd_2Fe_{14}B$ in the form of thin film presents the additional possibility of packing bits closer, using perpendicular recording where the spin representing the bits is oriented normal to the substrate, such applications are compared to micromagnetic devices requiring only small thickness films of about 20-50 nm [8].

CHAPTER 3

FABRICATION AND IMAGING TECHNIQUES

This chapter covers the theoretical background in this study in order to prepare hard magnetic thin film of neodymium- iron-boron and its characterization. Some techniques are employed here for both fabrication and imaging techniques.

3.1 SPUTTERING

Sputtering is the primary alternative to evaporation for metal film deposition in microelectronics fabrication, first discovered in 1852. Sputtering was developed as a thin film deposition technique by Langmuir in the 1920s. It provides better step coverage than evaporation and can produce layers of compound materials and alloys. These advantages here have made sputtering metal deposition techniques of choice for most silicon-based technology [10].

Sputtering is the process where atoms are released from the surface of a target material when it is bombarded by active ions. Sputtering is usually done by means of inert gases like Ar, meanwhile there is no chemical reaction between the sputtering gas and the target. The inert gas is ionized in a strong electric field, generating plasma above the target. When an incidental quantity of responsive gas such as oxygen or nitrogen is varied with the sputtering gas and released into the sputtering chamber through deposition, compound films of oxide or nitride can be prepared.This process is called reactive sputtering. When combined (multicomponent), most of this target can be prepared by the use of alloy films. Several sputtering systems are planned for thin-film deposition, including DC diode, RF diode magnetron and ion-beam sputtering [7].

3.1.1 Theory

A simple sputtering system, as in Fig. 3.1 is very similar to a simple reactive ion etch system with a parallel plasma reactor in vacuum chamber for sputtering deposition. Nevertheless, the plasma chamber must be prepared so that a high-energy ion strikes a target containing the material to be deposited. The target material, not the wafer, must be placed on the electrode expose with the maximum ion flux. To collect as many of these atoms ejected through the bombardments as possible, the cathode and anode in the sputtering system are closely spaced, often less than 10 cm. An inert gas is normally ionized and used to bombard the target materials. The gas pressure in the chamber is held at about 0.1 Torr. This results in a mean free path in the order of hundreds of micrometers [10].
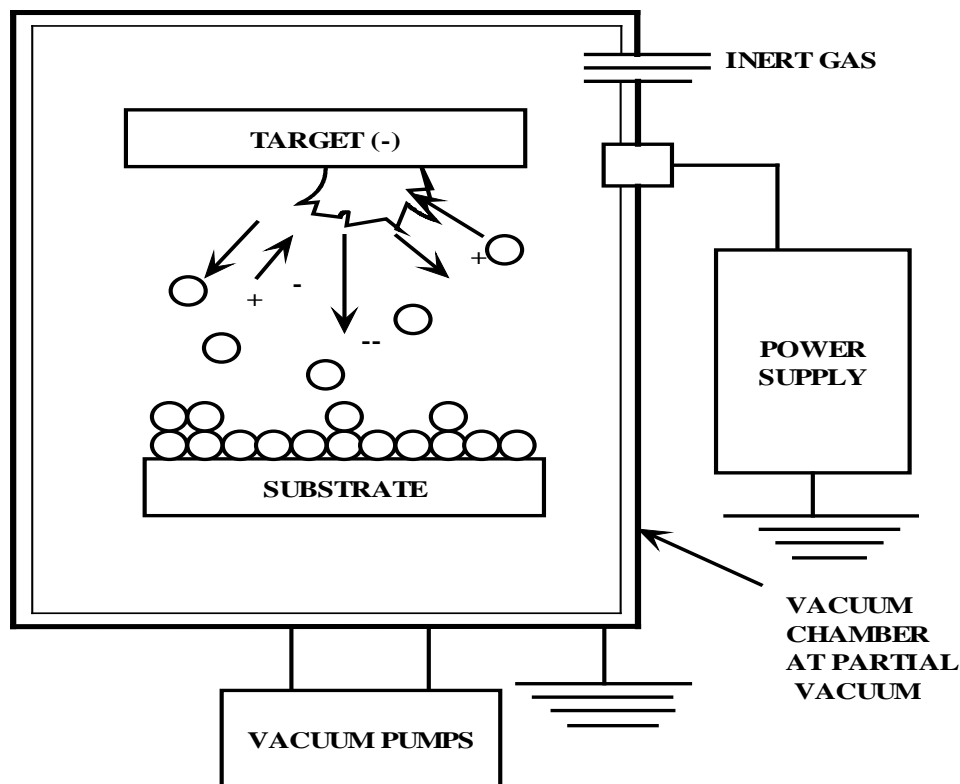

Fig.3.1 Sputtering vacuum deposition process [11].

3.1.2 Plasma

Glow discharges or plasma is introduced by applying a large voltage across a gap containing a low pressure gas. The required breakdown voltage is given by the following Paschen's law [10].

$$Vbd \propto \frac{PxL}{LogPxL+B}$$ (3.1)

Where P is the chamber pressure, L is the electrode spacing, and b is a constant. When the

plasma is formed, ions in the plasma are accelerated towards the negatively charged cathode. When they strike the surface, they discharge secondary electrons, which are accelerated away from the cathode. They may collide with neutral species; the atom can be excited state through an optical transition, provided that the characteristic glow and the energy transfer are high enough so that the atom will be ionized and accelerated towards the cathode. The bombardment of the cathode in this ion stream gives rise to the method of sputtering [10].

3.1.3 RF Sputtering.

In this study, RF sputtering is used, since it is usually performed at low gas pressure. In RF sputtering, the electrons acquired sufficient energy to cause ionizing collisions in the space between the plasma and electrode. When an RF potential with a large peak to peak voltage is capacitive coupled to an electrode, an alternative negative and positive potential appear on the surface. The electron reaches the surface to prevent any charge build-up. Since most of the bombarding energy produces heat by means of the large thermal gradient that can be generated [13]. Fig.3.2 a) shows some of the methods that may occur when an ion collides with a surface during the sputtering method. This near head-on collision may release a target atom that has a large momentum directed at a significant angle with respect to the normal surface. During this method, many of the bonds in the top layers of the target will be crushed if several of these large angle collisions occur; the incident atom or the recoiled target atom may change a significant velocity constituent parallel to the surface of the wafer [10]. A successive collision can then eject an atom or small clusters of atom as

shown in Fig.3.2 b). All surfaces visible to RF plasma change a negative prospective with respect to the plasma outstanding higher mobility of electrons than ions in the distinctive sputtering system, most of the voltage drop is on the target electrodes, but the bias on the substrate electrode leads to a bombardment of ions on the wafer. Regulating the DC bias on the electrode with respect to the plasma can regulate this effect. This has two major applications in microelectronics, sputtering cleaning and bias sputtering [12].
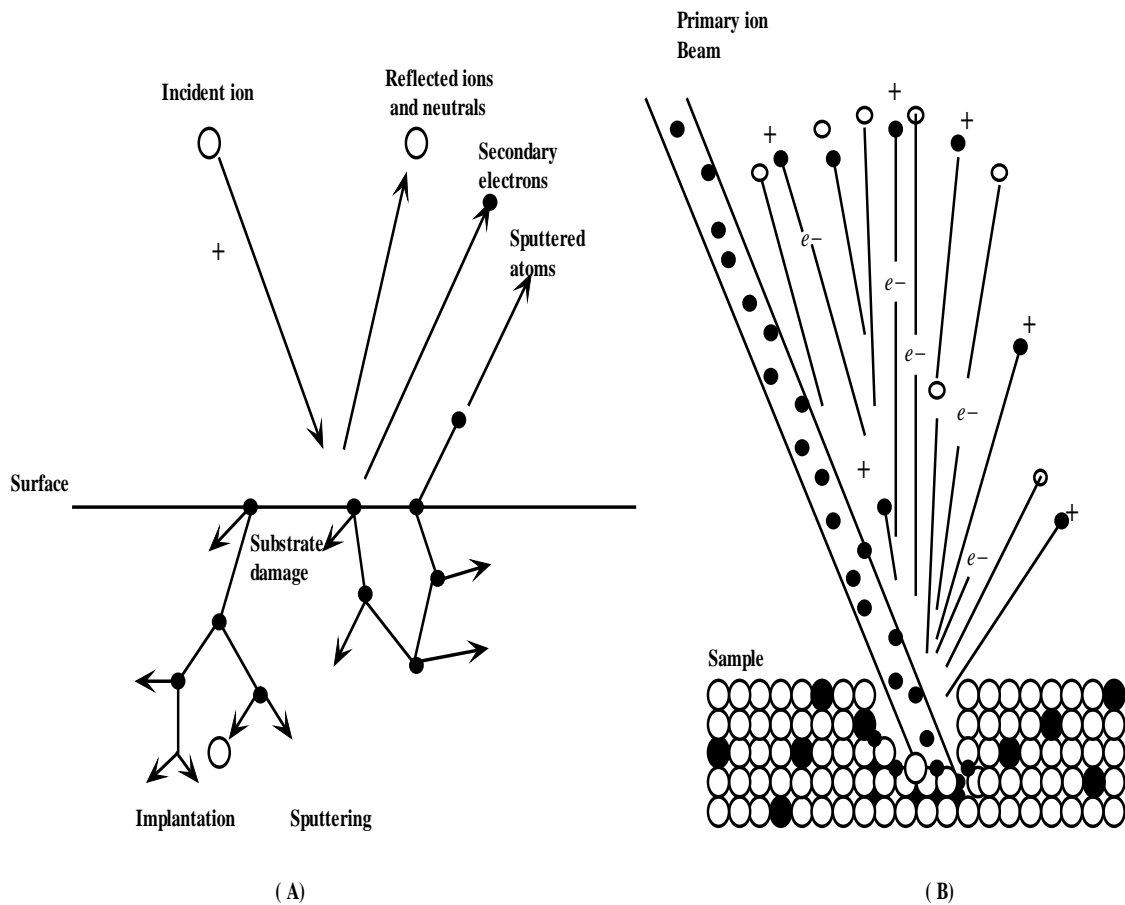

Fig.3.2 a) Possible outcome of an ion incident on the surface wafer [10]. b) Sputtering process [12].

3.2 THERMAL EVAPORATION

Thermal vacuum deposition is another method to fabricate thin films under a high vacuum environment also addressed as thermal evaporation method. With this method, an electron beam (E-beam) or resistive heating is usually used to evaporate the desired material inside the vacuum coating chamber, which then adheres to a substrate placed above it. This method can be classified as a form of PVD which stands for physical vapour deposition and is suitable for fabricating high quality thin films with thickness in the order of nanometers on glass, plastics, films, metals and almost any other kind of materials [14].

3.2.1 Resistively Heated Source

The best way of heating materials is to vaporize the material below 1500℃ by having contact with a hot surface that is heated when passing a current through a material (resistively heated). Evaporation sources must encompass a molten liquid without extensive reaction; the molten liquid must be kept away from falling onto the heated surface.This can be done either by means of a container such as a crucible, or by having moistened surface [15]. Fig.3.3 explains how the process of resistive chamber takes place as the temperature rises, thermal expansion causes the evaporator parts to move, this moment should be accounted for in the plan of the heater fixturing. Since metals expand on heating, the contacting clamps between the fixture and the source may have to be water-cooled to provide reliable clamping and contact resistance [13].
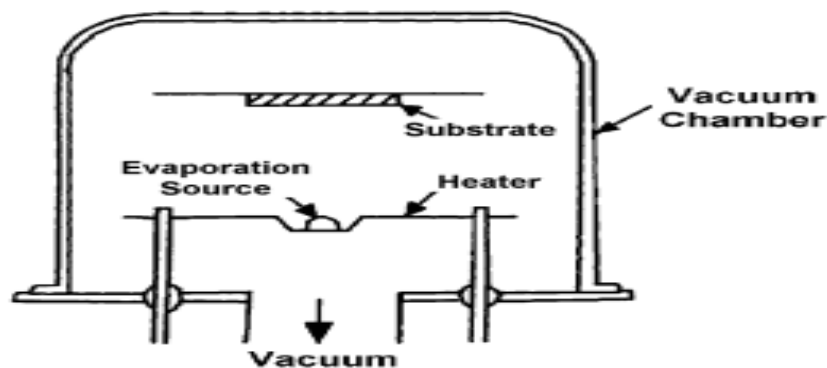

Fig.3.3 Resistive chamber [15].

3.2.2 Electron Beam Heated Source

Absorbed high energy electron beams are essential for the evaporation of intractable materials, such materials that absorb high energy are ceramics, glasses, carbon and deflecting metals. This ''e-beam'' heating is also suitable for evaporating large capacities of materials. Fig.3.4 shows when vaporizing solid surfaces of electrical insulating materials, local surface charge build-ups can transpire on the source surface leading to surface arcing that can produce particulate impurity in the depositing system. In the deflected electron gun, the high energy electron beam is designed by means of a thermionic-emitting filaments to create the electrons, high voltage (10 to 20 KV) to fast-track the electrons and electric or magnetic fields, to deflect the beam onto the surface of the materials to be evaporated [13] .
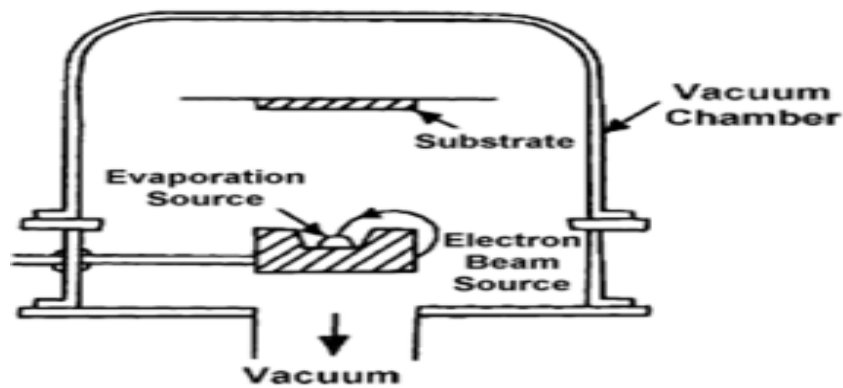
Fig.3.4 Electron beam chamber [13].

3.3 HALL-MICROMAGNETOMETRY IMAGING TECHNIQUES

Micromagnetometry encompasses a family of techniques that are used to evaluate local magnetic fields with a spatial resolution better than 100 µm in or on the surface of superconducting and magnetic samples. The techniques include Electron Microscopy (EM),

Magnetic Force Microscopy (MFM), Magnetic-Optical Imaging Microscopy (MO), Bitter Decoration, Scanning Hall-Probe Microscopy (SHPM), Scanning Superconducting

Quantum Interference Device (SQUID) Microscopy and a new scanning method named Scanning Josephson Junction Microscopy (SJJM).These methods differ in spatial resolution, field resolution and temporal resolution, i.e. the time needed to capture one image frame [16],[17],[18], [19], [20],[21].

3.3.1 Electron Microscopy (EM)

Electron Microscopy (EM) requires one to make a distinction between Lorentz microscopy and Electron holography. The former is an excellent technique for establishing the location of a magnetic object with a very high spatial resolution (about10nm) and modest sensitivity (about 1×10^{-3} T/$\sqrt{}$HZ). Moreover, since the output requires no post-processing, high-speed imaging in excess of video rates is possible [16].

3.3.2 Magnetic Force Microscopy (MFM)

Magnetic force microscope has been developed and introduced by Martin et.al. in 1987 [18], a year after the AFM has been developed. The initial MFM Probe was used with a sharpened iron or nickel wire to obtain a high resolution MFM image, the sputtered cobalt film on AFM cantilever and frequency modulating detection were used [19].

3.3.3 Bitter-Decoration Technique

The Bitter-Decoration method of imaging magnetic structures was developed in the 1930s. In this method, fine magnetic particles are dispersed on the magnetic structure by various techniques, including evaporation or use of liquid suspension. The magnetic particles deposit on the surface, and then imaged with an optical microscope or scanning electron microscope [20].

3.3.4 Atomic Force Microscope

Atomic force microscopy (AFM) is a novel technique for high resolution imaging of conducting as well as non-conducting surfaces. As shown in Fig. 3.5, the physical property sensed in AFM is the interaction force between the sample surface and a sharp probing tip. The cantilever detecting the atomic force is an essential element to significantly affect the spatial resolution of the AFM for high resolution imaging of the microscopic structure on

the sample surface, very sharp tip of the cantilever is required for fast imaging, and high mechanical resonant frequency of the cantilever is also necessary [21].
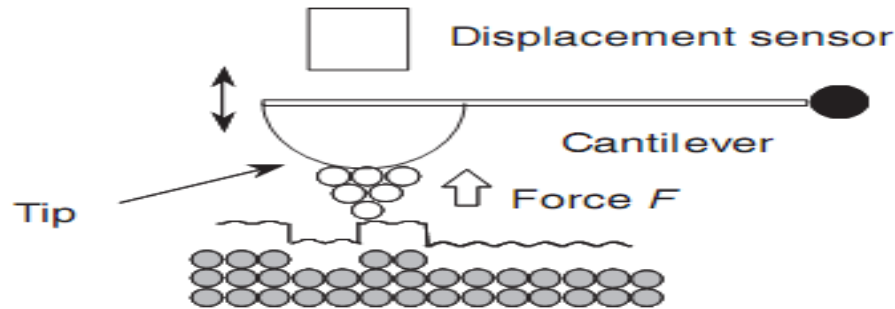

Fig.3.5 Schematic diagram of AFM [21].

3.3.5 Magneto-Optical Imaging (MO)

Magneto-Optical Imaging (MO) is also a mature technology which has a rather modest spatial resolution (about 1 µm) and sensitivity limited by the available MO materials and the need to bring them into intimate contact with the surface of the superconductors. The strength of this technique is in high-speed imaging, where modern pulsed lasers have made it possible to capture images at rates of 101 ns/frame with much faster acquisition with a real possibility [16].

3.3.6 Scanning SQUID Microscopy

Scanning SQUID Microscopy is a technique with the highest sensitivity less than 1×10^{-10} T/√HZ while the spatial resolution (about 4 µm) is limited by current micro fabrication capabilities and it seems certain to improve existing applications considerably underutilization of available signal-to-noise ratio (SNRs) and it is possible that scanning at video rates and beyond will be realized in the near future [17].

3.3.7 Scanning Josephson Junction Microscopy (SJJM)

Scanning Josephson Junction Microscopy extends the spatial resolution of scanning SQUID microscopy into the submicron scale. In a scanning joseph son junction microscope, a single Josephson junction is scanned across the surface of a sample. Local magnetic fields are detected by the modulation of the junction critical current. By using a sub-micron junction and a scanning tunneling microscope feedback system to maintain close proximity to the surface, a magnetic field sensitivity of 10^{-10}T with a spatial resolution 0.3 µm should be attainable for opening up new opportunities for imaging vortex configuration and the core structure in superconductors, as well as magnetic domains in magnetic materials [22].

3.3.8 Scanning Hall Probe Microscopy (SHPM)

In this study, we employ Low Temperature Scanning Hall Prove Microscopy (LTSHPM) for the unique set of advantages and excellent spatial resolution. The first scanning Hall probe microscope with a sub-micron Hall probe was developed by Chang et.al [16], [17]. While this system had an excellent spatial resolution (about 0.35 µm), its field resolution of 3.6×10^{-5}T/$\sqrt{\text{HZ}}$ at 300 K was rather poor, which demanded very slow image acquisition. Simple improvements in Hall probe design by Oral et.al [23] led to a considerable improvement in sensitivity of several orders of magnitude and allowing for high-resolution images to be captured at about 1 frame/s with a measurement bandwidth of 1 KHZ.

Scanning Hall Probe Microscopy (SHPM) is a powerful non-invasive quantitative method for investigation of magnetic properties of samples where the sample is scanned with the Hall probe in close proximity to its surface. Fig. 3.6 shows a schematic layout of a state- of the-art scanning Hall probe microscope [24]. The Hall probe is mounted on the piezoelectric scanner tube of a commercial low-temperature scanning tunneling microscope with a stick slip coarse approach mechanism and tilted $1 \div 2^{0}$ with respect to the sample [16], [24].
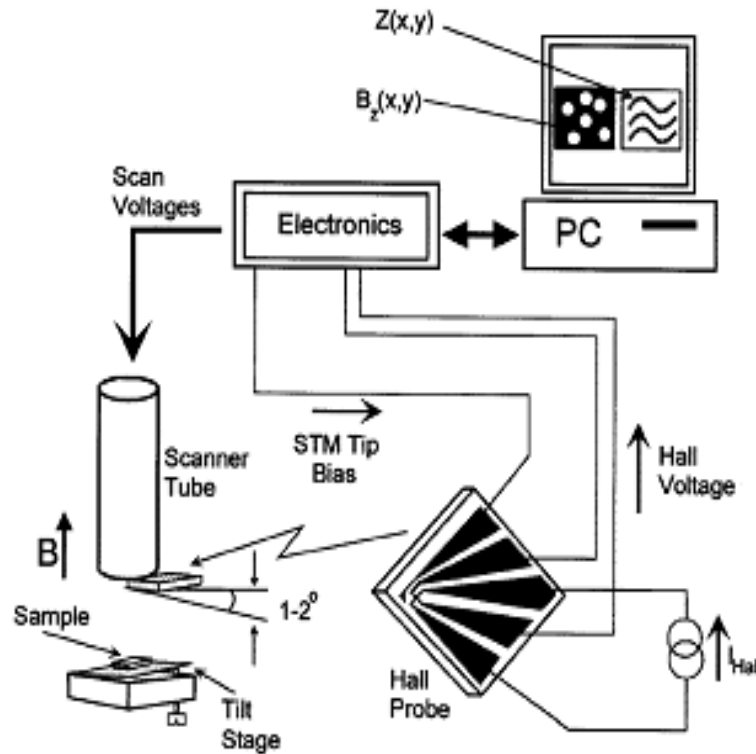
Fig.3.6 Schematic diagram of a scanning Hall probe microscope [24].

Fig.3.7 shows the schematic diagram of a scanning electron micrograph of a typical 2DEG Hall probe of 0.8μm resolution.The requirements are fulfilled with a micromagnetometry technique that usually uses a Greek-cross-shaped Hall probe based on heterostructures with two-dimensional electron gas (2DEG). Several new techniques based on Hall probe sensors have been developed for the observation of magnetic fields over ferromagnetic and superconducting samples in the past decade [16].

Fig.3.7 Electron micrograph of a Hall probe with 0.8 µm spatial resolutions [16].
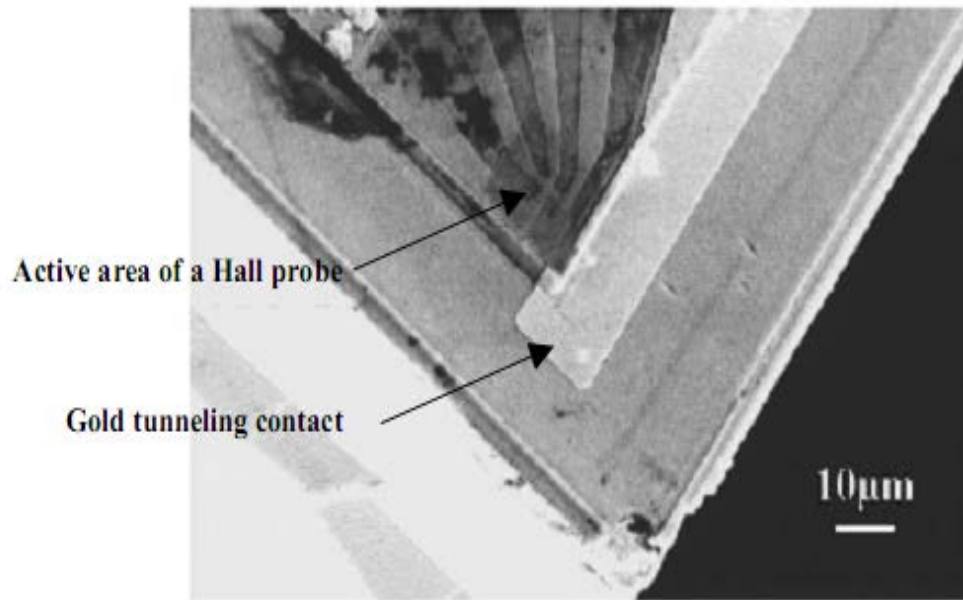
The SHPM can work in two modes: The STM tracking mode in Fig. 3.8 a) and the Flying mode in Fig.3.8 b). In the tracking mode, the sample is approached until tunneling is established and the Hall probe is scanned across the surface to measure the magnetic field and surface topography simultaneously. In the flying mode, the sample can be retraced by a fraction of a micron and the Hall probe is scanned much more rapidly with a slightly lower spatial resolution. Before commencing flying SHPM, it is usual to measure the scanner plane and sample tilt angles with the scanning tunneling microscope tip so that this can be electronically compensating during scanning.This is the preferred mode of SHPM operation since it is fast and avoids the risk of a head crash often encountered during the much slower scan with STM tracking mode [16].
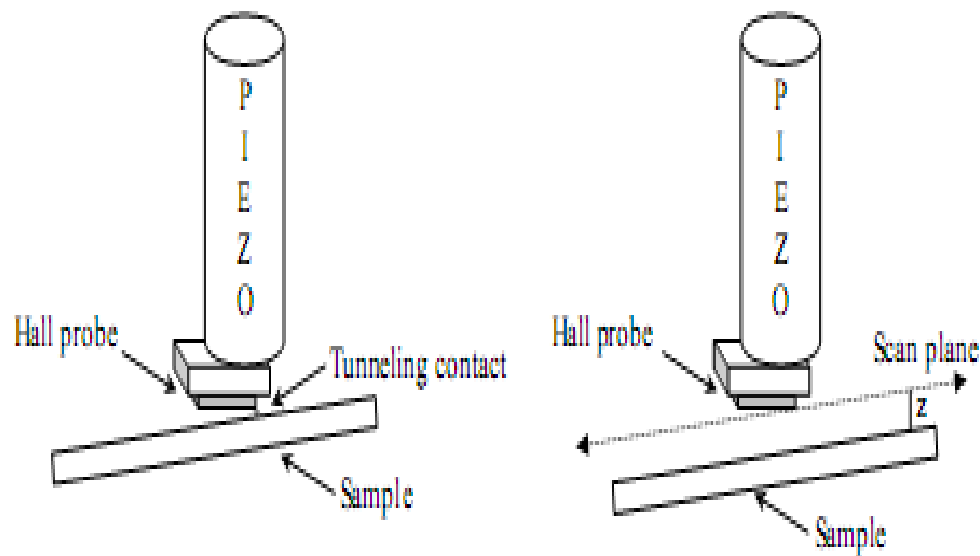
Fig.3.8 Diagram illustrating a) The STM mode and b) The Flying mode of SHPM [16].

SHPM techniques provide a unique set of advantages over its counterparts as described below:

- This technique measures the magnitude of the Z-component of the magnetic field [25].
- Excellent field resolution can be achieved in the presence of a large applied magnetic field ($7x10^{-6}T/\sqrt{HZ}$ at 300 K and $6x10^{-9}T/\sqrt{HZ}$ at 4 K [26].
- Imaging is possible in a wide temperature range ($300\ mK - 340\ K$) [29].
- Relatively short scan time of ($\approx 1\ sec$) makes dynamic magnetic imaging possible [29, 30].
- Spatial resolution as high as (50 nm) can be achieved [27].
- Scan area as large as (1 cm) can be achieved [28].

3.3.9 High Field Scanning Hall Probe Imaging

The principle is to limit the point of a Teflon slider, so that the Hall sensor is mounted by two steel arms XY plane as seen in Fig. 3.9. The scan can be rotated around its vertical axis, thereby causing the slider to move around the plane. The connecting steel rod is to monitor the movement of the X and Y rotation. Therefore, the driving motors can be distant from the scanning plane to keep it at room temperature and the sample is dipped in liquid nitrogen.The whole scanner is shown schematically in Fig.3.10 [31].
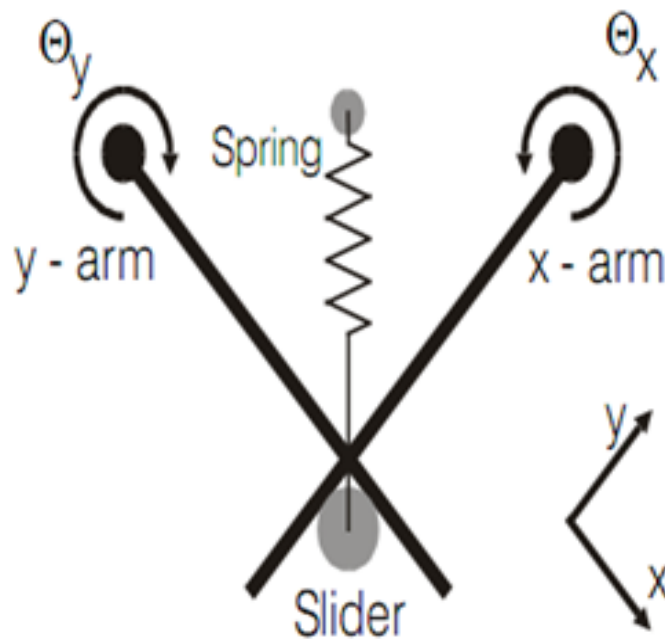
Fig.3.9 The design concept of a high field scanning Hall probe microscope [31].

In Fig.3.10, a pivot is used here for the suspension of the Hall sensor at the top of the apparatus. The scanning surface is in circular form truly not flat, but sphere-shaped with 80 cm radius. The sphere-shaped alteration and any disorder of the sample are compensated during the scan process. The Z- coordinate is being controlled by a third motion position.

The plane of contact is established for both the sensor and sample by means of a capacitive strain gauge mounted on the sensor. This brings proximity to the Hall probe of the sample (10 µm). The sensor is a 50 µm Hall bar patterned from 1.5 µm Insb on GaAs which has a sensitivity of $1x10^{-6}T/\sqrt{HZ}$ over a temperature range of $20 \div 300$ K and field range of $0 \div 20$ K [30].
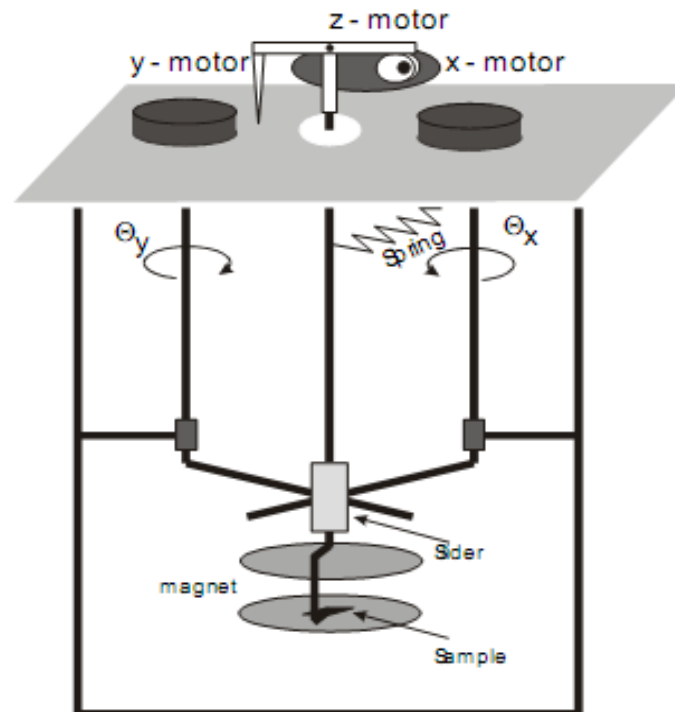
Fig.3.10 Diagram of the scanner and the cryostat in a high field scanning Hall probe microscope [31].

The highest scanning area is approximately 10×10 mm^2 with a step size ~ 25µm and repeatability 10µm.The highest stepping speed is currently 300 steps/sec. The time taken to measure an image is of order 10 minutes. The probability to source a sample and quality at DC and AC frequency level is the advantage of this system [31].

CHAPTER 4

EXPERIMENTAL PROCEDURE

Study shows that the fabrication of Nd-Fe-B thin films were firstly demonstrated by Cadieu, Cheung and Wickramasekara 1986.They prepared Nd-Fe-B films using a slow deposition rate together with applying bias field in the in-plane direction and high H_c of 16 KOe was achieved. However, in order to consider a practical use, some drawbacks were pointed out. The substrate temperature during deposition, 750 ℃ was too high and the easy magnetization axis was aligned in the in-plane direction, since then, many studies have been made in order to control the crystal orientation and to improve the magnetic properties [7].

In this report, intensive work and research were carried out for the sample fabrication; the topographical image of the sample surface and the domain were conducted in the Material Science and Engineering Laboratory in Meliksah University, while the X-ray diffraction analysis were both performed in UNAM, Bilkent University, Ankara and Meliksah University.

The system that we used during fabrication has a two stage-vacuum system with a roughing-mechanical pump and a high vacuum turbo pump.The system is first evacuated down to E^{-2} Torr using the roughing mechanical pump, and then the turbo pump is employed to pump the chamber down to E^{-8} Torr during the whole process.The mechanical pump used for roughing is also to back the turbo pump for removal of exhaust gas. This system has liquid nitrogen to trap the impurities of the system as in Fig.4.1

.

Fig. 4.1 Vacuum chamber for deposition process

4.1 SAMPLE FABRICATION

Samples were prepared by RF sputtering from home-made Nd-Fe-B target as in Fig.4.2a and a target of Mg was used to remove oxygen from silicon substrate at room temperature condition in a vacuum system with a base pressure of $2\text{x}10^{-7}$ Torr. Deposition was performed in ArH (%5) gas mixture with 4.5 mTorr chamber pressure. CuTEM with 1500 square-mesh was used as a shadow mask to pattern the film as shown in Fig.4.2b. Pre-sputtering was introduced to clean the target for an hour before sample deposition started.
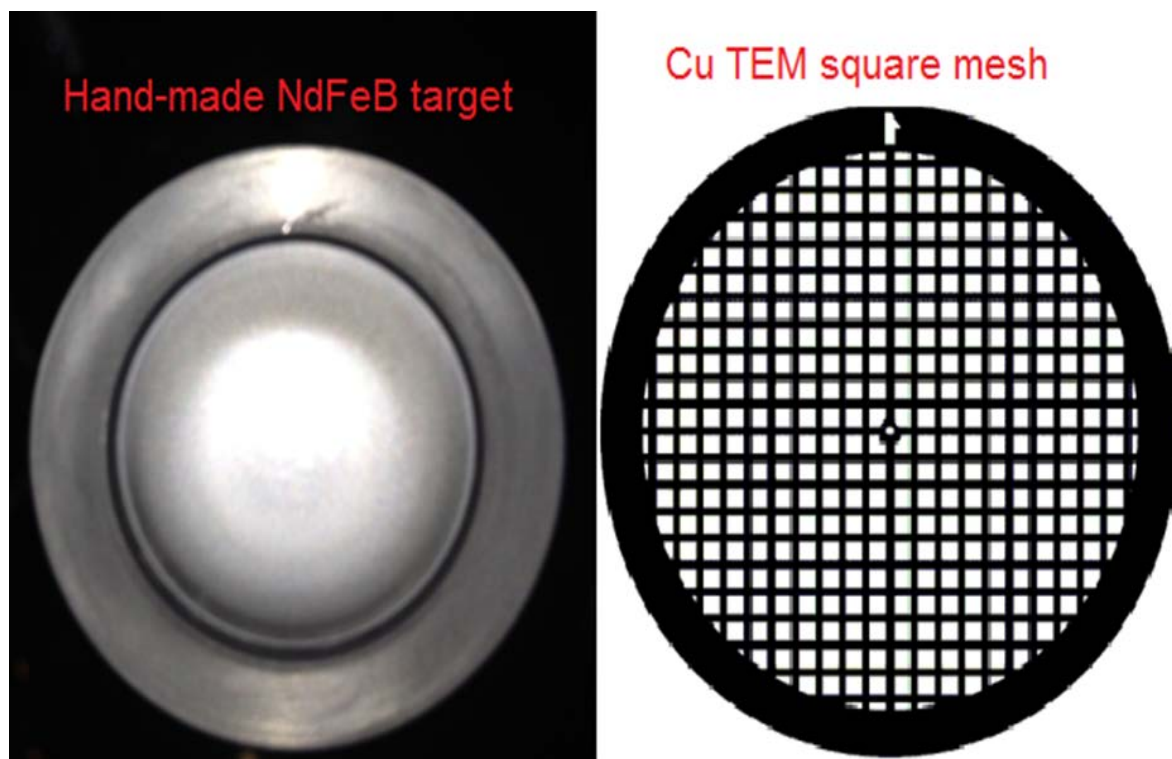
Fig.4.2 a) Home-made Nd-Fe-B target. b) Cu-TEM square-mesh

Samples with layer of 260 nm thickness were prepared separately for annealing and then deposited. In order to keep the Nd-Fe-B film free from diffusion and oxidation, a 10 nm thick tantalum (Ta) capping layer was deposited, since it has a high absorption rate for residual gases. 4.5 Torr was used during the sputtering process and the deposition rate for Nd-Fe-B was 0.5 Å/s with the substrate to target distance held at 10.0 cm. The deposition rate was monitored every 10 minutes and records were kept to ensure that the deposition rate reached to its final thickness of the film. The liquid nitrogen cold finger was added periodically during the sputtering process to ensure trapping of the impurities in the system and easy phase formation of the film material thereby forming a nitride or oxide. Following the fabrication process, films were thermally annealed at 550 ℃ for 30 minutes under vacuum condition as in Fig.4.3. The thermal heating chamber consists of a long Quartz tube flushed with pure Argon gas and was subsequently evacuated down to about E^{-3} Torr before the annealing begins. The sample film was placed on a copper plate for thermal

uniformity and inserted into the tube. Annealing process was critical to acquire $Nd_2Fe_{14}B$ films with large coercivity.Formation of $Nd_2Fe_{14}B$ phase largely depended on the annealing temperature and duration. Films were annealed in home-made rapid thermal annealing system. Heating and cooling rates were approximately 30℃ per second.

Fig.4.3 Thermal heating chambers

Furthermore, a rapid thermal annealing system was used in UNAM, Bilkent University in order to realize thermal heating with N_2 atmosphere. This system refers to semiconductor manufacturing process which heats silicon wafer to high temperature in order to affect its electrical properties. During cooling, however, wafer temperature must be brought down slowly to prevent dislocation and wafer breakage due to thermal shock.Wafer can be heated in order to activate dopant change film to film or film to wafer substrate interface, density of deposited film changes the state of grown films.

However, in this process we carried out the annealing process, firstly the annealing atmosphere was purged with N_2 at 500 sccm flow rate for 5 minutes. Following this, under N_2 atmosphere with a flowing rate of 100 sccm. We heated the annealing environment up to 550 ℃ at ramp rate of 9.17 ℃/sec for 1 minute. The samples were annealed for 30 minutes under these conditions. After annealing process was completed, the sample was cooled down to 0 ℃ at ramp rate of 18.33℃/sec for 30 seconds.The annealing atmosphere was purged with N_2 at 500 sccm flow rate for 10 minutes, and the process was finalized.

X-ray diffraction pattern was performed for the formation of $Nd_2Fe_{14}B$ and its lattice orientation. Furthermore, a low temperature scanning Hall probe microscopy system which has different tracking modes is to be used in obtaining the tropical image of the sample surface.

Deposition material:

Nd-Fe-B, Mg Targets

 Substrate: Silicon Wafer

 Base pressure: $2x10^{-7}$ Torr

Thickness: 260nm

 Temperature: Room Temperature

Table 4.1. The results obtained during deposition process.

Time (min)	Thickness KÅ	Deposition rate(Å/s)	Chamber pressure(Torr)	Current I(A)	Voltage V(V)	Ar Flow W	RF W
11.00	360	0.5	$5.5E^{-3}$	0.056	256	40	70- 17
20.00	640	0.5	$6E^{-3}$	0.053	265.4	40	70-18
30.00	975	0.6	$6.75E^{-3}$	0.053	256.4	40	70-18
50.00	1730	0.6	$7E^{-3}$	0.052	256.4	40	70-18
65.00	2250	0.6	$7E^{-3}$	0.051	256.4	40	70-18
75.00	2600	0.6	$7E^{-3}$	0.051	256.4	40	70-18

4.2 SCANNING OF SAMPLE SURFACE OF NdFeB THIN FILM

A low temperature SHPM system as in Fig.4.4 [32] is used with the purpose of scanning the sample surface at high temperature during the experimental procedure. The idea is to scan the sample surface and examine it applying the hall cross sensor directly onto it. The Hall sensor was mounted directly on the piezotube of a low temperature scanning Hall probe with a stick slip coarse approach mechanism. The Hall sensor is situated or adjusted in such a manner that the corner of a deep etch mesa is the highest position of the tip. As the tip is scanned above the sample surface, some magnetic force, which acts on the tip, tends to deflect the cantilever.

Fig.4.5 shows how the sample is tilted to angle approximately $1^0 - 1.25^0$ with respect to the Hall probe chip and is positioned on the corner of the cantilever. During the experimental setup, care must be taken because the Hall probe is a delicate one which can be easily damaged. The Hall sensor starts scanning across the sample surface with the aid of piezoelectric crystal, and if the sample surface is rough, it causes the cantilever to bend. Piezoelectric crystal is used for both coarse approach in the Z direction and fine scanning on X-Y-Z. An automatic approach can be used in order to avoid the probe from crashing to the sample surface. The movement in X-Y plane is controlled by piezoelectric crystal so that for each X-Y-Z coordinate, the data is automatically recorded during the scan and stored as information in the matrix. The images are 3D images in scanning probe microscopy techniques, for each X-Y coordinate, there is surface property measurement. This surface property data can be a height for scanning tunneling microscopy techniques (STM) and atomic force microscopy (AFM) or can be a magnetic field strength for scanning Hall probe microscopy (SHPM) techniques. The scan is usually performed slowly, line by line and the data is taken for both forward and backward motion.

Fig.4.4 Observing the Hall probe-sample surface angle with a microscope Courtesy of
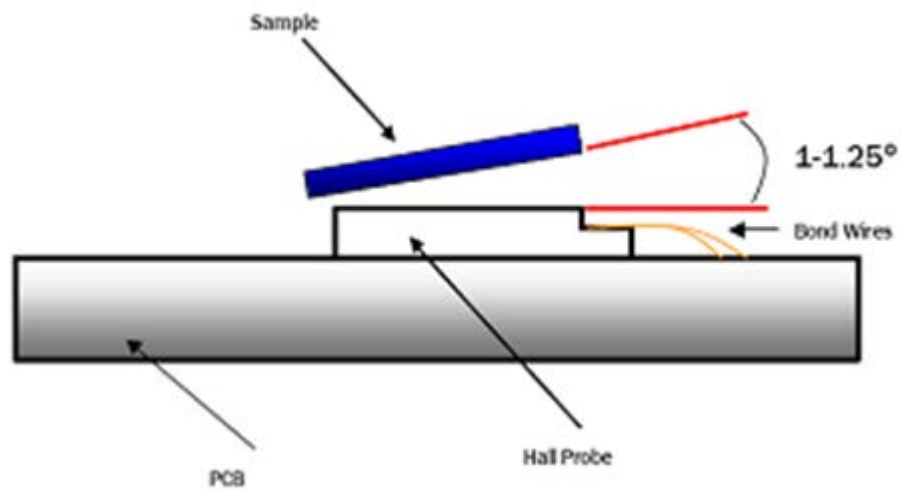Nanomagnetic instruments inc. (http://web.nanomagnetic-inst.com) [33].

Fig. 4.5 The proper angle between Hall probe chip and sample surface Courtesy of
Nanomagnetics instruments inc. (http://web.nanomagnetics-inst.com) [33].

CHAPTER 5

RESULTS AND DISCUSSION

5.1 X-RAY DIFFRACTION PATTERN

X-ray diffraction is an extremely powerful tool in the field of material characterization to obtain information on an atomic scale from both crystalline and noncrystalline material. This technique can be used to get structural information about thin film and lattice orientation. Diffraction analysis was done for both non-annealed and annealed temperature and to identify the crystalline phase present. The degree of grain size and texture are important parameters for $Nd_2Fe_{14}B$ and it is, therefore, the major phase in our sample to determine the magnetic behavior.

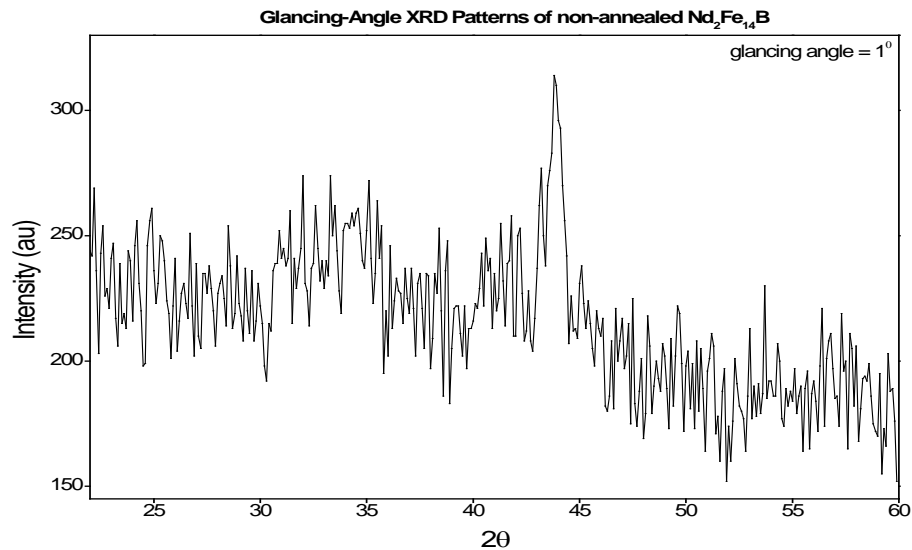The XRD pattern of non-annealed NdFeB film after deposition is shown in Fig. 5.1 and 5.2.

Fig.5.1 Non-annealed $Nd_2Fe_{14}B$
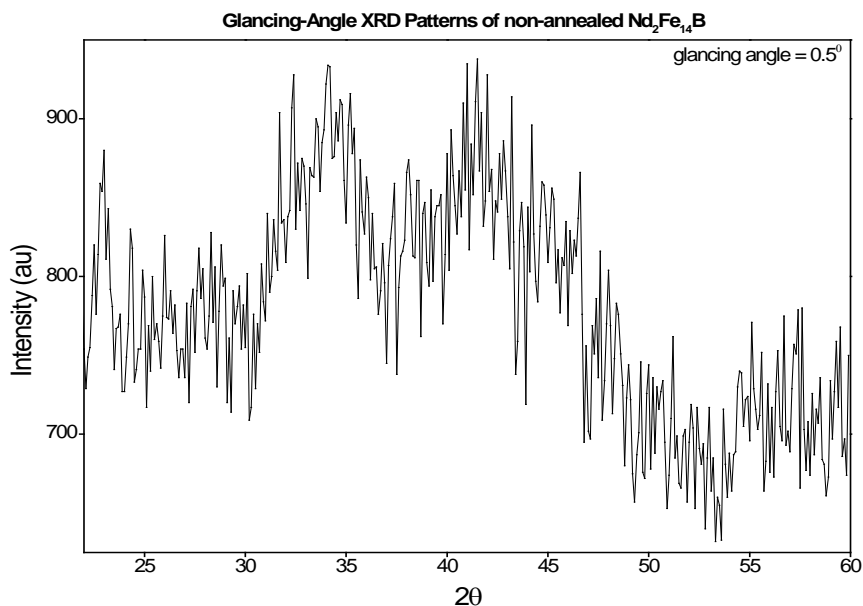
Fig.5.2 Non-annealed $Nd_2Fe_{14}B$

The non-annealed type of Nd-Fe-B film pattern's results do not display any diffraction peak for the formation of $Nd_2Fe_{14}B$ phase, but rather show the evidence of large number of suppressed peak display at two different glancing angles of 1^0 and 0.5^0 as seen in both Fig 5.1 and 5.2, which show the presence of magnetic layer amorphous of Nd-Fe-B after deposition at room temperature. The film was amorphous since it did not require to undergo any transformation effects and we, therefore, concluded that the formation of $Nd_2Fe_{14}B$ phase largely depends on the annealing temperature and duration of time. Similar observations were made by Leo.K.E.B and et. al in [34].

The XRD pattern of the NdFeB film annealed at 550°C for 30 minutes after deposition is presented in Fig. 5.3 and 5.4
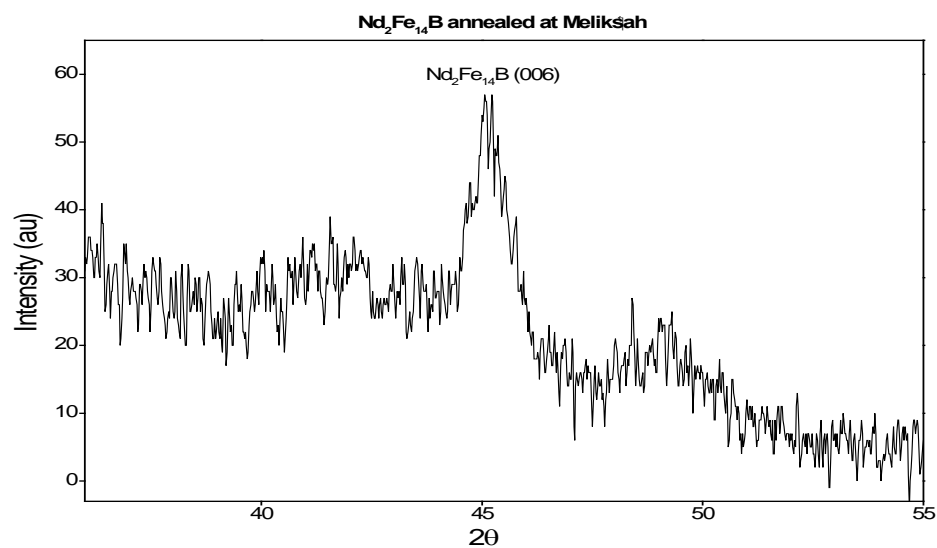

Fig.5.3 $Nd_2Fe_{14}B$ annealed at 550°C for 30 minutes

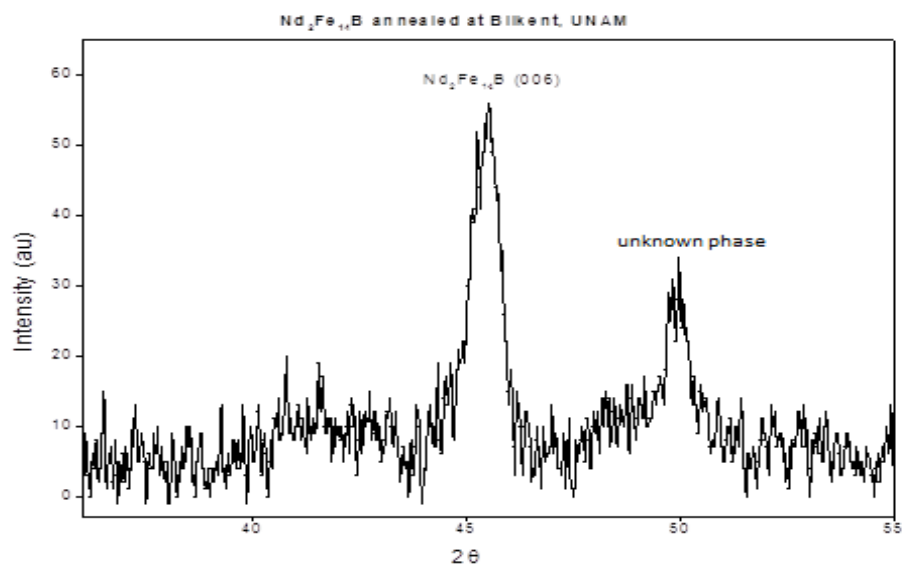Fig.5.4 $Nd_2Fe_{14}B$ annealed at 550°C for 30 minutes

The result in Fig. 5.3 was obtained in Meliksah University, and Fig. 5.4 results were obtained in UNAM Bikent University. The results both show the formation of $Nd_2Fe_{14}B$ phase at critical peak intensity with (006) orientation, which show the main peak. The X-ray diffraction data shows some evidences of rocking curve at various intensity with the selection of the 2θ points as base background for determination of the accurate integrated peak intensities measured at critical peak. It can also be seen in Fig.5.4 that the peak intensity of $Nd_2Fe_{14}B$ (006) peak is much stronger than that of the unknown phase peak, which is slightly a nitride phase since it was annealed in N_2 and suppressed. Hence, the greatly enhanced peak is (006) ($2\theta \approx 45\theta$) reflection of $Nd_2Fe_{14}B$ which shows a perfect c-axis texture in the film and is perpendicular to the plane. However, annealing temperature at 550℃ for 30 minutes has been reached out, since the film underwent a structural transformation from amorphous to crystalline structure, and the prominent peak was identified as corresponding to$Nd_2Fe_{14}B$. We have shown that the formation of $Nd_2Fe_{14}B$ is one good thing to have high coercivity and saturation magnetization. Annealing temperature and annealing time have played a vital role in developing magnetic thin film with high coercivities. The results obtained from X-ray diffraction analysis data have the following implications: Because the crystallization of $Nd_2Fe_{14}B$ can only occur when annealing temperature Ta $\geq$ 500℃ is less than 627℃, crystallization temperature of $Nd_2Fe_{14}B$ phase. This is reasonable because the crystallization temperature decreases when Nd concentration increases [35].

5.2 SCANNING RESULTS OF OUR SAMPLE SURFACE DEPOSITED BY A HOME-MADE NdFeB FILM ANNEALED AT 550℃ FOR 30 MINUTES

The results obtained here have played a vital role for the scanning of our sample surface by extracting information about the topographical profile of magnetic field strength (B) across the sample, which were acquired by scanning Hall probe microscope (SHPM), scanning tunneling microscope (STM) and atomic force microscope (AFM). It is often more effective to employ the non-contact mode in order to prevent the sample surface and the probing tip getting in contact with the surface, and thus, frequency shift is made to

maintain the space between the probing tip and the sample surface. The following parameters were chosen to scan the images of our sample during image processing with the scanning Hall probe. These parameters include the scan area set of interest measured in micrometer, the image size, which identifies any individual bit in pixels, the scan speed measured in micrometer that counts the number of cycles in seconds, and the change in frequency shift measured in hertz.

The scanning results of our sample surface are shown in Figure 5.5, 5.6 and 5.7, acquired by a scanning tunneling microscope (STM) tracking mode to ensure a high resolution image and image of height constant mode. The results show the topographical image of our sample surface, the cross section line paths of the selected dots which show how it behaves in nature and its three dimensional view in X,Y and Z directions. The image has also shown the cross section of our shadow mask with 1500 square-mesh that patterns the film surface. It can be seen that some noise takes place on the sample surface because of the sensitivity of the tunneling gap to temperature implication.
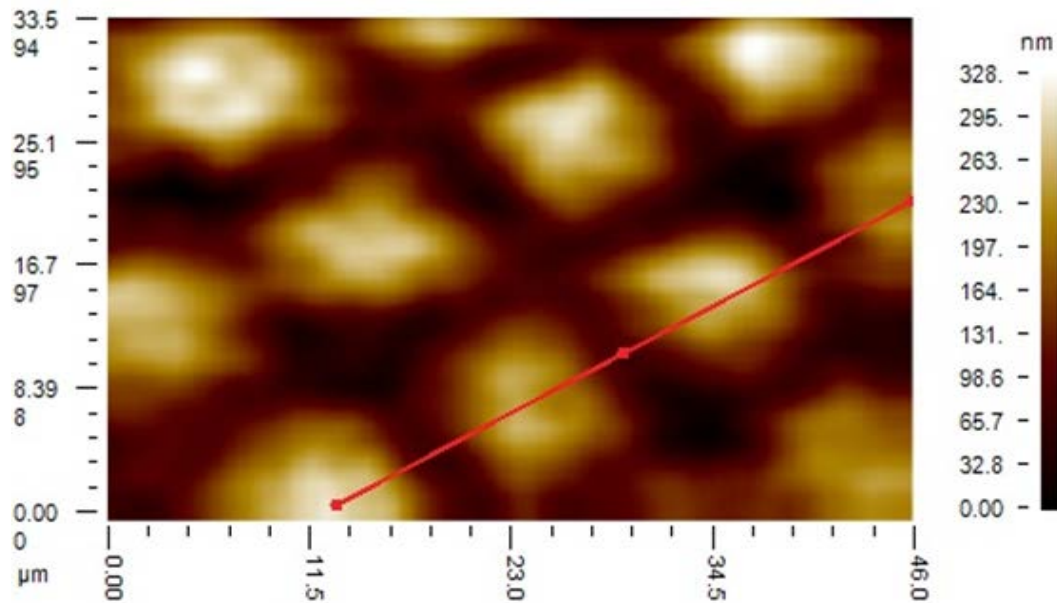

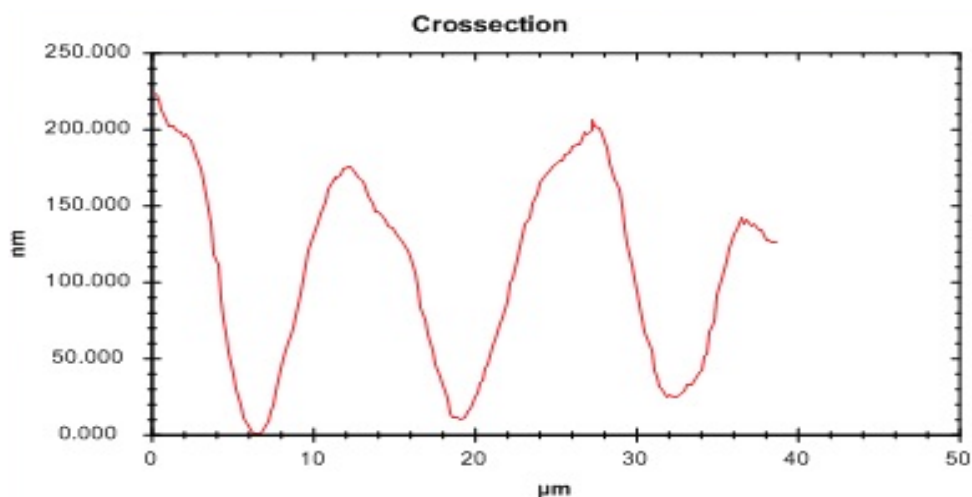Fig.5.5 Topographical image of NdFeB pattern dots at 300 K

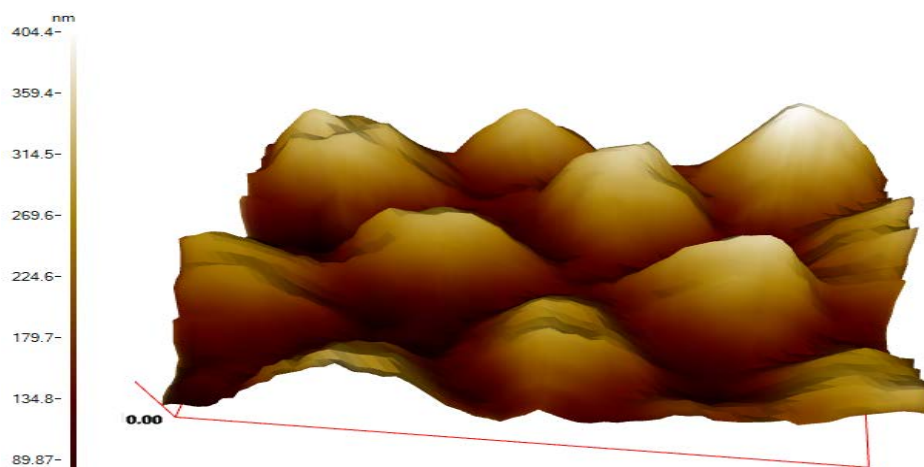Fig.5.6 Cross section line paths of selected pattern dots at 300 K

Fig.5.7 3D view of the image sample by STM

The results above can be achieved through the set of scan parameter's value so that smooth image as well as the topographical profile of magnetic field distribution is established with 30 µm/s scan speed. The scan area is limited within the substantial area for a sharp image and the image size is taken over 33.5 µm by 46.0 µm resolution in pixels. We set the first hall coefficient of 0.0089 Ω/Gauss at 300 K followed by the hall coefficient of 0.0129 Ω/Gauss at 150 K down to a hall coefficient of 0.0164 Ω/Gauss at 10 K, which gives information about the high resolution at various stages of temperatures

effectively. We have chosen the best image at 300 K among the temperatures reading. The hall current was set to be 5 μmA with a gain parameter of 1 and bandwidth of 0.1 KHZ.

The scanning results of our sample surface are shown in Figure 5.8, 5.9 and 5.10, acquired by scanning Hall probe microscope (SHPM) to ensure high resolution image as well as smooth image. The results show the topographical image of our sample surface, the cross section line paths of the selected dots, which show how it behaves in nature and its three dimensional view in X,Y and Z directions. The image has also shown the cross section of our shadow mask with 1500 square-mesh that pattern the film surface. It can be observed or seen that the appearance of our sample surface, the image are smooth and well complimented as a result of low external vibration and drift stability.
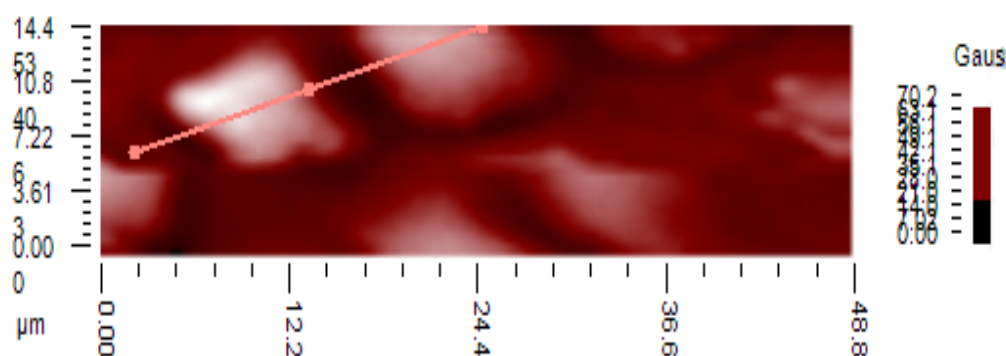

Figure 5.8 Topographical image of NdFeB Pattern dots at 300 K
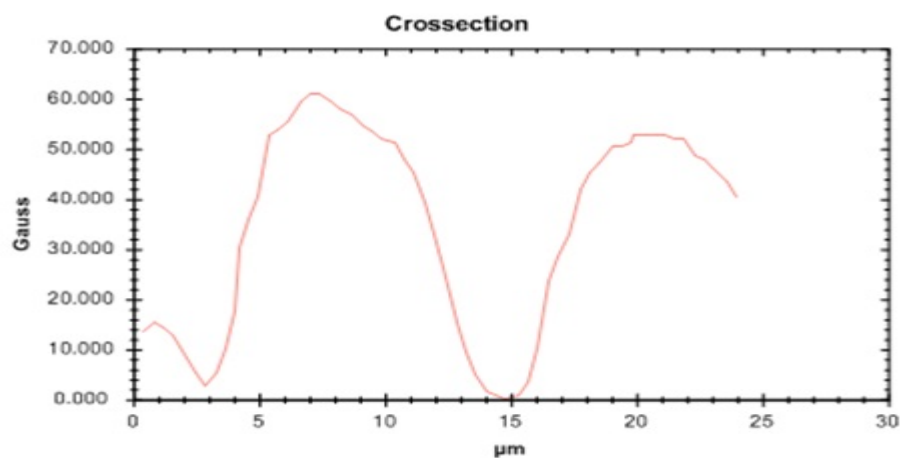

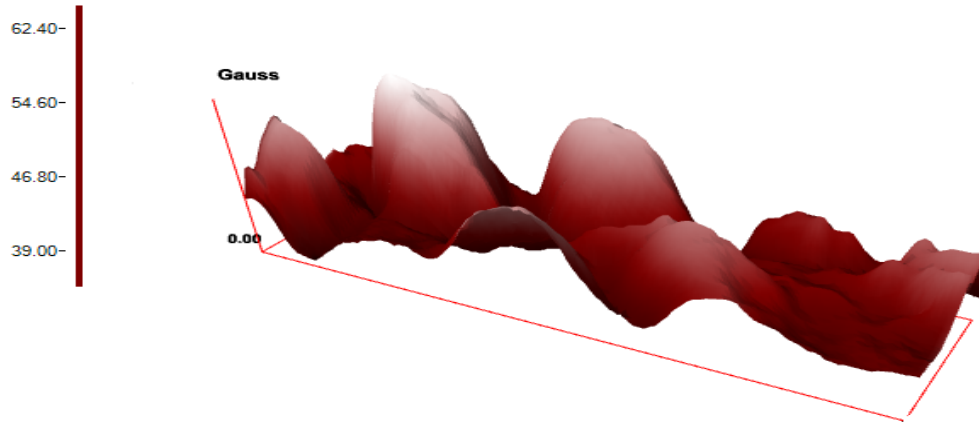Fig.5.9 Cross section line paths of selected pattern dots at 300 K

Fig.5.10 3D view of the image sample by SHPM

The results above can be achieved through the set of scan parameter's value so that smooth image as well as the topographical profile of magnetic field distribution is established with 20 µm/s scan speed. The scan area should be within the limit area for a sharp image scan and the image size is taken over 14.4 µm by 48.8 µm resolution in pixels, but during scan process, the tip gets crashed into the sample surface. We set the first hall coefficient of 0.0089 Ω/Gauss at 300 K followed by the hall coefficient of 0.0129 Ω/Gauss at 150 K down to a hall coefficient of 0.0164 Ω/Gauss at 10 K, which gives information about the high resolution at various stages of temperatures on our sample surface effectively, and we have chosen the best image sample among the temperature readings. The hall current was set to be 5 µmA with a gain parameter of 1 and bandwidth of 0.1 KHZ.

Scanning results of our sample surface are shown in Figure 5.11,5.12 and 5.13, acquired by atomic force microscope (AFM) tracking mode to ensure topographical image with smooth surface at high resolution. The results show the topographical image of our sample surface, the cross section line paths of the selected dots, which shows how it behaves in nature and the three dimensional view in X,Y and Z directions. The image has also shown the cross section of our shadow mask with 1500 square mask that pattern the sample surface. It can be seen that some noise occurs on the sample surface as a result of uncontrolled random fluctuation of the voltage across the devices and external vibration.
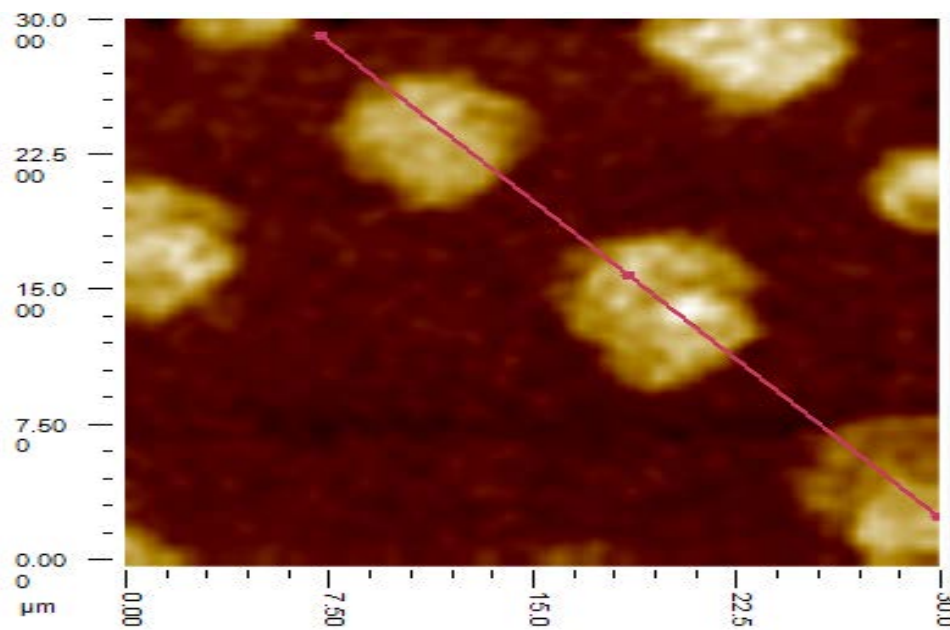
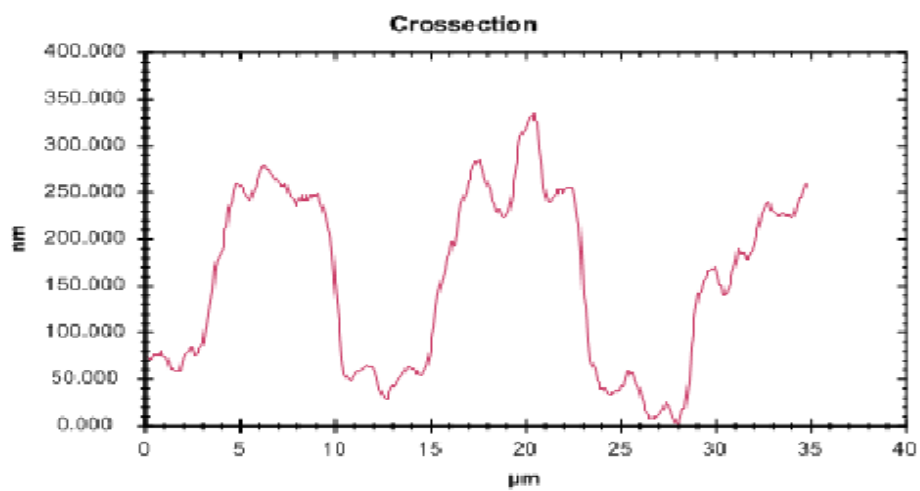Fig.5.11 Topographical image of NdFeB pattern dots at 300 K

Fig 5.12 Cross section line paths of selected dots at 300 K
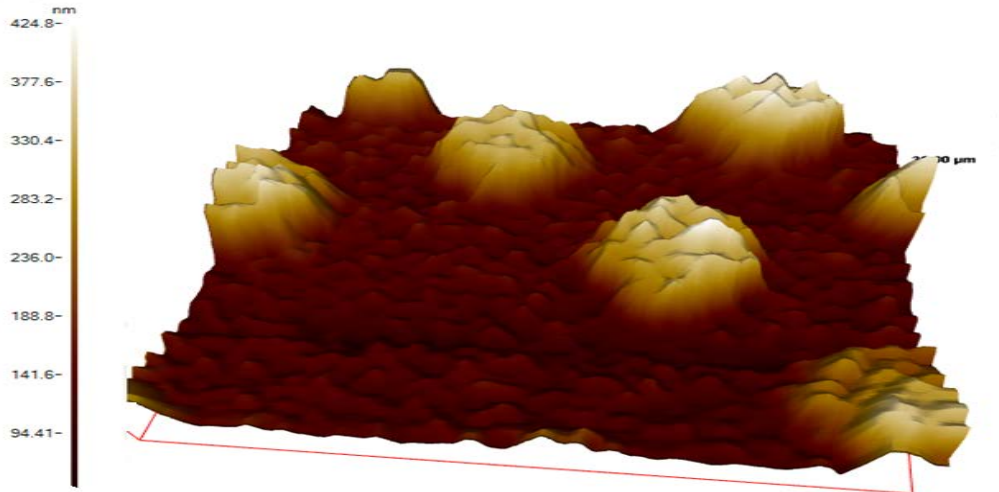
Fig.5.13 3D View of the of the image sample surface

The results above can be achieved through the set of scan parameter's value so that smooth image as well as the topographical profile of magnetic field distribution is established with 25 μm/s scan speed. The scan area should be within the considerable area for a sharp image and the image size is taken over 30 μm by 30 μm resolution in pixels. We set the first hall coefficient of 0.0089 Ω/Gauss at 300 K followed by the hall coefficient of 0.0129 Ω/Gauss at 150 K down to a hall coefficient of 0.0164 Ω/Gauss at 10 K, which gives information about the high resolution at various room temperature on the sample surface effectively, and we have chosen the best image sample at 300 K among the temperature readings. The hall current was set to be 5 μA with a gain parameter of 1 and bandwidth of 0.1 KHZ.

CHAPTER 6

CONCLUSION

In this study, we fabricated Nd-Fe-B thin film with thickness of approximately 260 nm on silicon substrate and a target of Mg was used to remove oxygen from silicon substrate at room temperature condition. Cu TEM with 1500 square mesh was used as a shadow mask to pattern the film surface. Films were capped with few nanometer thick tantalum layer against oxidation and diffusion. The films were thermally annealed at 550 ℃ for 30 minutes. X-ray diffraction pattern was performed for both non-annealed and annealed temperature as grown sample, and formation of Nd_2Fe_2B film was confirmed by the use of X-ray diffraction analysis results at critical peak intensity.

We have imaged the sample surface with the aid of the low temperature SHPM system to be used for obtaining the scanning image of the sample surface at various temperatures which are acquired by different tracking modes to establish the high resolution image as well as the topographical profile of magnetic field distribution to be achieved. The image results then show that the scanning images with SHPM give high resolution image and are well complimented with its counterpart results of atomic force microscope (AFM) tracking mode and scanning tunneling microscope (STM) tracking mode. The films which were studied will be used for applications in superconductor and ferromagnetic hybrid systems.

APPENDIX

LOW TEMPERATURE SCANNING HALL PROBE MICROSCOPY

This section covers the experimental setup instruments and assembly that we carried out during the experimental investigation with the aid of the low temperature scanning Hall probe (LT-SHPM). The following figures were used during the experimental setup and procedure.

Fig. 5.14 shows how sample is mounting. A spring loaded screws are used to place the X-Y slider puck on the sample slider after the sample surface is set, making sure the entire arrangement is clean and dry. Avoid the use of bare hands for low temperature application [36].
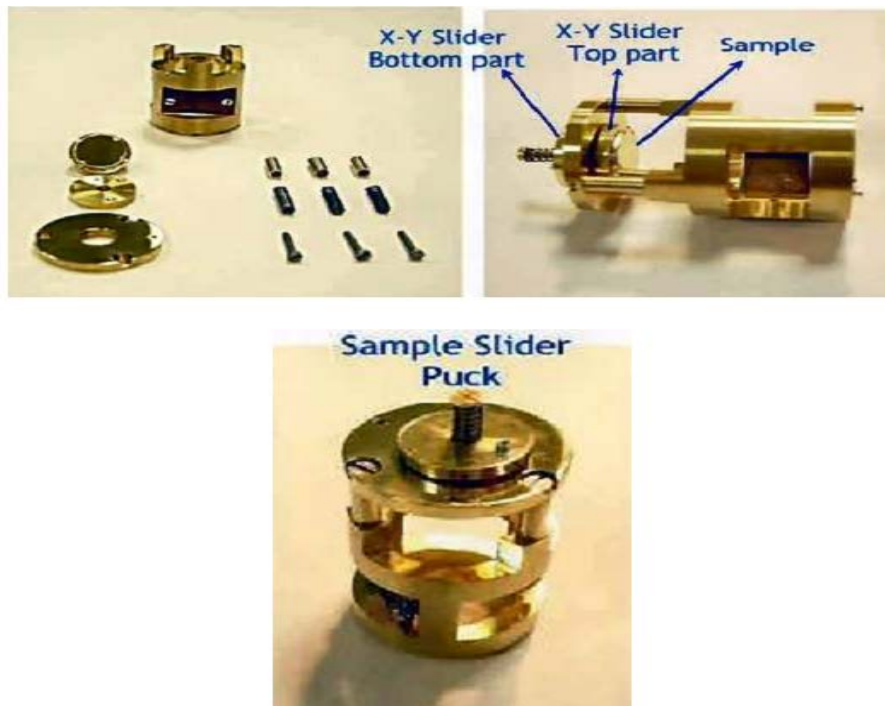

Fig.5.14 Sample slider puck and X-Y slider puck assembly Courtesy of Nanomagnetic instrument inc. (http://web.nanomagnetics-inst.com) [33].

Fig.5.15 Quartz slider tube cleaning Courtesy of Nanomagnetic instruments inc.
(http://web.nanomagnetics-inst.com) [33].

Fig.5.15 shows the quartz slider tube cleaning. Acetone is used to clean the Hall probe and the quartz tube after the Hall probes should be rinsed with isopropanol and made well dried, an appropriate cleaning cloth is used to wipe the quartz tube. Care must be taken while handling Hall probe in the ultrasonic bath and drying it. Lesser power operation is advisable for the soncater [36]. In order to mount the Hall probe on microscope, the microscope is suspended upright on the wooden stand. Fig.5.16 shows how to successfully mount the Hall probe on the microscope. An aluminium shield is placed above the quartz tube for protection and the Hall probe is installed on the scanner head with a pair of screw sets. Avoid trying the screw too much. Next, the gold coated brass coil tube can be installed before the sample slider assembly is fixed to position the Hall probe, which should be checked to ensure proper function [36].
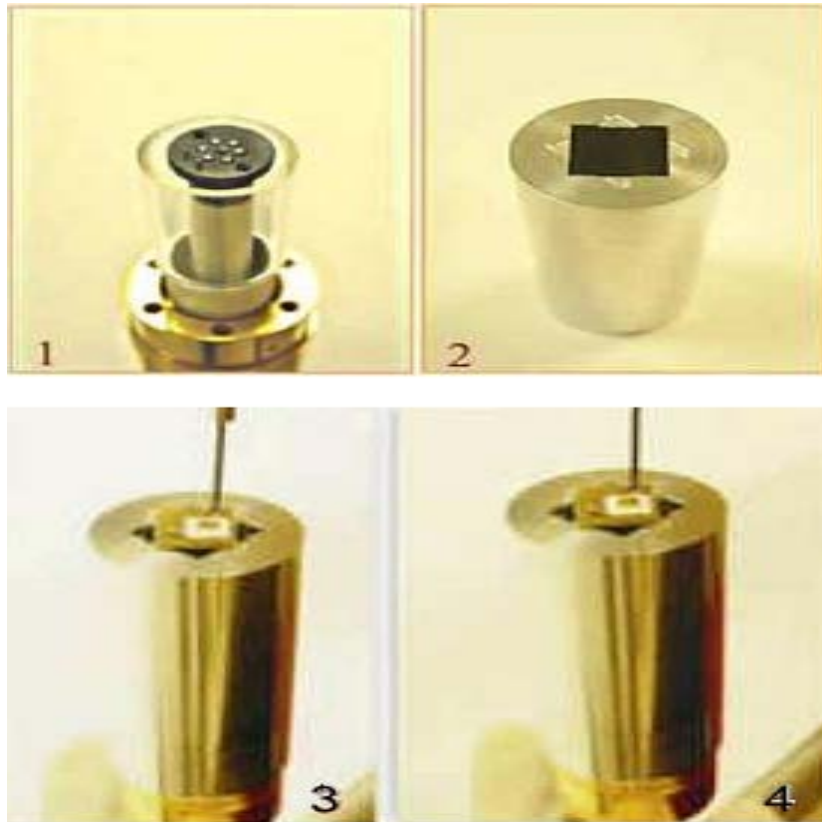
Fig.5.16 Mounting Hall probe on scanner head, Courtesy of Nanomagnetics instruments inc. (http://web.nanomagnetics-inst.com) [33].

Fig.5.17. After the ''checked Hall probe'' feature is selected in the SPM software, the electronic applies a 10 volt sinusoidal signal to the coil. An oscilloscope is used to monitor the Hall voltage response and the original signal. A powerful permanent magnet can be placed close to the Hall probe. The Hall voltage can be checked by agitating the permanent magnet pole. Fig.5.17 and 5.18 show how to remove the brass shield. After registering a Hall probe signal, the brass shield should be removed to install the sample slider puck. The sample slider should be inserted with much care to avoid crashing it. Damages to the Hall probe can be irreversible. One of the three sets of screws in the sample slider puck needs to be aligned with Hall probe chip diagonal. This practice makes the sample-Hall probe arrangement very simple without applying extra force, and use the fingertip to tighten the brass slim leaf as much as possible without applying extra force [36].

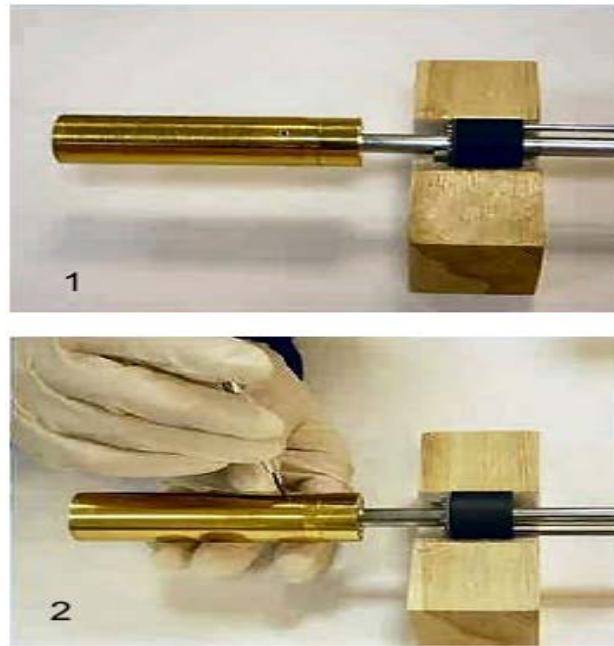Fig.5.17 Brass coil and shield assembly 1-2 Courtesy of Nanomagnetics instruments inc.

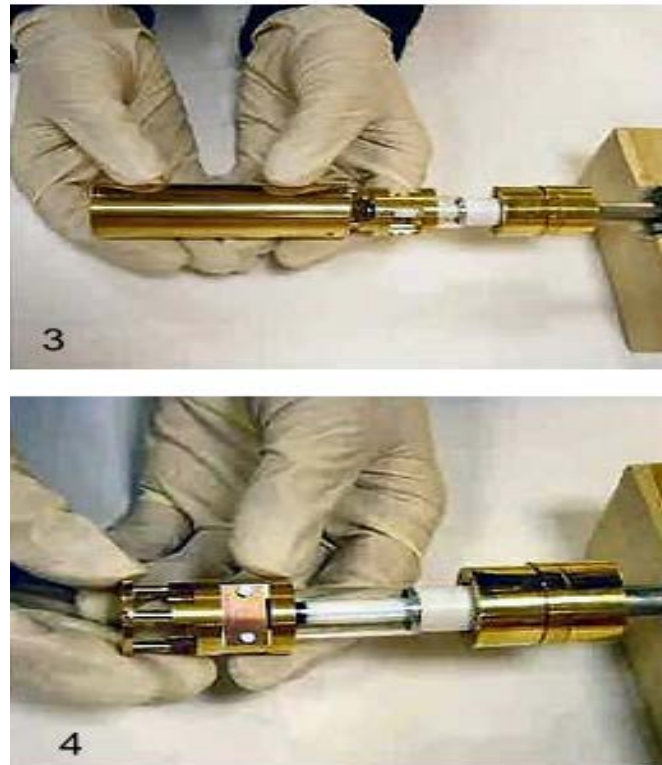(http://web.namagnetics-inst.com) [33].

Fig.5.18 Brass and coil shield assembly 3-4 Courtesy of Nanomagnetics instruments inc.

(http://web.nanomagnetics-inst.com) [33].

Fig.5.19 shows the complete view of LT-SHPM unit; the system is sensibly placed in the PPMS so that seal and purge are performed by several cycles. An automatic approach can be used in order to avoid Hall probe tip getting in contact with the surface. The user should observe the tunneling signal and function of the SPM software. The response speed of the feedback loop is determined by the set of value during the approach. Several steps are taken to realize the tip position in the negative or positive direction of Z and the step should be kept within the range of 250, not above. During the cooling of the sample, it creates physical vibration and therefore, the hall probe should be withdrawn the step by the automatic retract option [36].
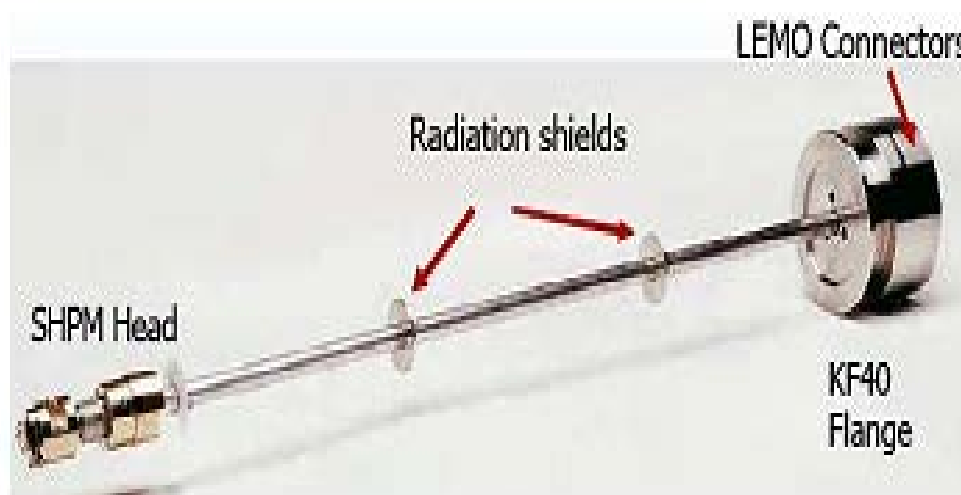
Fig.5.19 Complete view of LT-SHPM unit Courtesy of Nanomagnetics instruments inc. (http://web.nanomagnetics-inst.com) [33].

This section describes the electronic circuit unit as in Fig.5.20, which interfaces with the computer software that are used to drive, control and acquire data from the scanning probe microscope. Basically, the circuit consists of the following components. The scanning circuit, which provides the signal for the scanning the tip over the sample surface. The function generator, which drives the tunning fork at certain amplitude and frequency, can be controlled by the phased loop. It was also used for pre-amplifier which amplifies the output signal for the tunning fork sensor and the control loop which is used to boost the sensitivity or depress the scanning speed [36].
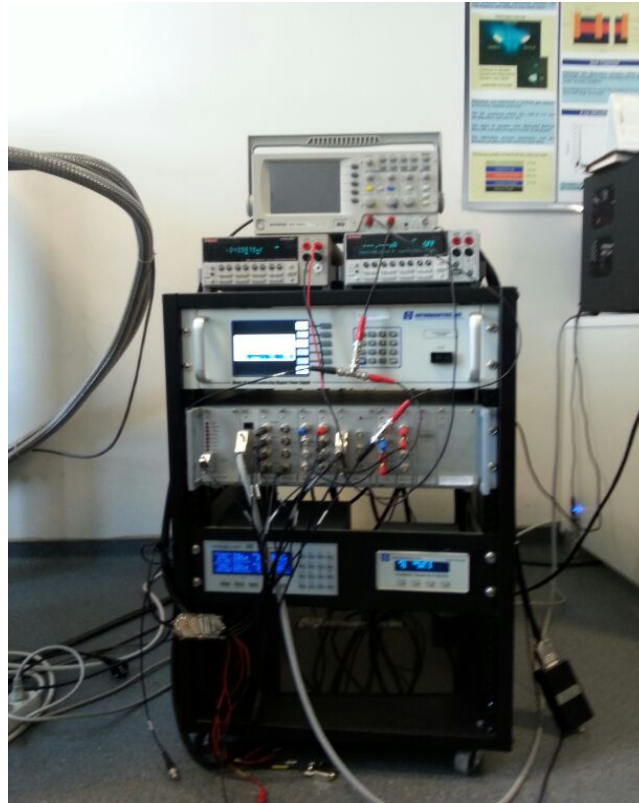
Fig.5.20 Electronic control unit for scanning probe microscope Courtesy of Nanomagnetic instruments inc. (http://web.nanomagnetics-inst.com) [33].

Fig.5.21 describes the superconducting magnet system which is the system that comprises of cryostat, integrated variable temperature and software control system. The system has solenoid design for 90 kilo gauss (9.tesla) at 4.2 K with a +/-0.01 homogeneity over 1 centimeter. A system established on a close loop helium expansion cycle is a cryogenic system. The system has two leading components, namely the compression packages which are used to tighten the refrigerant and extract heat from the system and secondly, the cold head, through which supplementary expansion cools down to cryogenic temperature using the refrigerant. 99.99% pure helium will be the refrigerant gas used in the cryogenic system [33].

Fig.5.21 Nanomagnetic inc.LT-SHPM 1.5-320 K cryomagnetics inc. 9 tesla dry cryostat Courtesy of Nanomagnetic instruments inc. (http://web.nanomagnetics-inst.com) [33].

Compressed helium is now transported by a flexline stainless steel line called helium flexline from the compressor package to the cold head and low-pressure helium is transported back. The way it meets expectations is that pure low-pressure helium returned from the cold head is compressed by an oil lubricated compressor. Then, the head of the compressor is detached from heat exchanger. Oil separator and filter are now used to remove the oil from the compressor. After that, by the use of a high pressure helium flexline, the compressed helium is then given to the cold head. The variable temperature insert uses a continous flowing gas source, which is cooled to less than 2.0 Kelvin by heat exchanger attached to the cryocooler. The computer software control system is attached interfaces to drive, control and acquire data from the scanning probe microscope [33].

REFERENCES

[1]   W. Rodewald, "Rare-Earth-Transition-Metal Magnets," in *Handbook of Magnetism and Advanced Material*, pp. 1907-1937, John Wiley, Oxford, 2007.

[2]   W. Szmaja, "Investigation of the Domain Structure of Anisotropic Sintered Nd-Fe-B-base Permanent Magnets" , *Journal of Magnetism and Magnetic Material,* Vol.301, pp. 546-561, 2006.

[3]   J. Jeremey Anderson, *Structural and Magnetic Properties of Neodymium-Iron-Boron Cluster*, MS.Thesis, Nebraska University, 2010.

[4]   F. Xu, F. Yang, X. Ping and et.al,''Microstructure Characterization of High Energy-Product NdFeB Thin Film''*Process in Natural Science*, Vol.20, pp.76-80, 2010.

[5]   W. D. Calister and D. G. Rethwish, *Material Science and Engineering*, John Wiley, Asia, 2011.

[6]   B. D. Culity, *Introduction to Magnetic Material*, John Wiley, New York, 2011.

[7]   T. Shima and K. Takanashi,''Hard Magnetic Films'', in *Handbook of Magnetism and Adavanced Material*, pp.2234-2236, John Wiley, Oxford, 2007.

[8]   C. Constantinescu and N. Scarisoreanu,''Thin Films of NdFeB Deposited by PVD Techniques'',*Applied Surface Science*, Vol.253, pp.8192-8196, 2007.

[9]   C. Constantinescu, E. patroi and M. Codescu,''Effect of Nitrogen Environment on NdeFeB Films grown by Radio Frequency Plasma Beam assisted Pulsed Laser Deposition'', *Material Science and Engineering*, Vol.178, pp.267-271, 2013.

[10]   S. Campbell, *Science and Engineering of Microelectronic Fabrication*, University Press, Oxford, 2001.

[11]   ''What is Sputtering'', TCB-Thermal Conductive Bonding, 2010. http://www.tcbonding.com/sputtering.html.

[12]   ''Secondary Iron Mass Spectrometry Theory Tutorial'' Islamic Azad University-PPRC Plasma Physics Research Center, 2012. http://www.pprc.tripod.com/SIMs/Theory.html

[13]   D. Mattox,''Physical Sputtering and Sputter Depostion''*, in Handbook of physical Vapor Depostion (PVD) Processing,* pp.237-305, Elsevier, Oxford, 1998.

[14]   J. Koskinen,''Thermal Evaporation'', in *Comprehensive Material Processing*, pp.4-55, Elsevier, Finland, 2014.

[15]   D. Mattox,''Evaporation and Vacuum Deposition'', in *Handbook of Physical Vapor Deposition (PVD) Processing*, pp.195-237, Elsevier, Oxford, 2010.

[16]   S. J. Bending,''Local Magnetic Probes of Superconductors'',*Advance in Physics*,Vol.48, pp.449-535, 1999.

[17]   H. Bluhm,''Magnetic Field above the Surface of a Superconductor with internal Magnetism'',*Physical Review*,Vol.76, pp.14507-7, 2007.

[18]   Y. Martin and H. K.Wickramasinghe,''Metallic Films for Electronic, Optical and Magnetic Application'',*Applied Physics Letter*,Vol.50, pp.1455-1457, 1987.

[19]   S. Hosaka,''Magnetic Force Microscope'', in *Road Map of Scanning Microscope*, pp.67-75, Springer, New York, 2007.

[20]   F. Bitter,''Spin Polarized Scanning Electron Microscopy'',*Physical Review*,Vol.38, pp.1903-1905, 1991.

[21]   Y. Sugawara,''Atomic Force Microscopy'', in *Road Map of Scanning Microscope*, pp.32-38, Springer, New York, 2007.

[22]   B. L. T. Plourde,''Design of Scanning Josepphson Junction Microscope on Microscope for Submicron-Resolution Magnetic Imaging''*,Review of Scientific Instruments*,Vol.70, pp.4344-4347, 1999.

[23]   A. Oral, *Scanning Hall Probe Microscopy Quantitative and Non-Invasive Imaging and Magnetometry of Magnetic Material at 50 nm Scale*, Springer, New York, 2007.

[24]   A. Oral, ''Real Time Scanning Probe Microscopy'',*Applied Physics Letter*, Vol.69 (9), pp.1324-1326, 1996.

[25]   U. Hartmann, Scanning Probe Method for Imaging, Springer, New York, 2005.

[26]   S. Mitchell, ''Electrical Magnetic and Optical Properties of Material'', in an introduction to Material Engineering and Science, pp.285-307, John Wiley, New Jersey, 2003.

[27]   A. Sandhu, K. Kurosawa, M. Dede and A. Oral,''50 nm Hall Sensor for Room Temperature Scanning Hall Probe Microscopy'', *Japanese Journal of Applied Physics,* Vol.42 (2), pp.777-778, 2004.

[28] R. B. Dinner, M. R. Beasley and K. A. Moler, ''Cryogenic Scanning Hall Probe Microscope with Centimeter Scan range and Sub-micron Resolution'', *Review of Science Instruments*, Vol.76, pp.1037-1039, 2005.

[29] A. Oral, J. C. Barnard, S. J. Bending and T. Moltenni,''Direct Observation of Melting of the Vortex Solid in $Bi_2Si_2CaCuO_8$'', *Physical Review Letter*, Vol.80 (16), pp.2613-3610, 1998.

[30] M. Dede, A. Oral, T. Yamamoto, K. Kadowaki and H. Shritrikman,''Real Time Imaging of Vortex-antivortex annihilation in $Bi_2Si_2CaCuO_8$ to single Crystal by Low Temperature Scanning Hall Probe Microscopy'', *Japanese Journal of Applied Physics*, Vol.45, pp.2246-2250, 2006.

[31] G. K. Perkins,''High Field Scanning Hall Probe Imaging of High Temperature Superconductor''*IEEE Transaction on Applied Superconductivity*, Vol.11, pp.3186-3189, 2001.

[32] R. AKram,''Variable Temperature Scanning Hall Probe Microscopy with GaN/AlGaN Two Dimensional Electron Gas (2DEG) Micro Hall sensor with 4.2-42 K range using quartz tunning fork AFM Feedback''*, IEEE Transaction on Magnetics*, Vol.44, pp.3255-3259, 2008.

[33] *Low Temperature Scanning Hall Probe Microscope (LT-SHPM) Mannual*, NanoMagnetic Instruments Ltd, Oxford, 2006.

[34] L. K. E. B. Serrona, A. Sugimura and et.al,''Magnetic and Structural Properties of NdFeB Thin Film Prepared by Step annealing'', *Material Science and Engineering*, B97, pp.59-63, 2003.

[35] M. Yu, Y. S. Hwang Liou and D. J. Sellmyer,''Nanonstructured NdFeB Films Processed by Rapid Thermal annealing'', *Journal of Applied Physics*,Vol.82 (11), pp.6611-6618, 1998.

[36] A. E. Ozmetin, *Magnetic Imaging of Micrometer and Nanometer-size Magnetic Structures and their Flux-Pinning Effects on Superconducting Thin Film*, PhD Dissertation, Texas A&M Univerisity, 2009.